Chinese Journal of Chemical Engineering 88 (2025) 108–123

Contents lists available at ScienceDirect

Chinese Journal of Chemical Engineering

journal homepage: www.elsevier.com/locate/CJChE

Full Length Article

Hydrogen production from biomass waste gasification under the enhancement of catalyst-sorbent hybrid functional material synthesized from steel slag

Zechen Zhang [1], Tanzila Anjum [1], Yinxiang Wang [1], Yucen Meng [1], Tianheng Qin [2], Ye Shui Zhang [2], Yutao Zhang [3], Aimin Li [1], Guozhao Ji [1,*]

[1] *Key Laboratory of Industrial Ecology and Environmental Engineering, School of Environmental Science and Technology, Dalian University of Technology, Dalian 116000, China*
[2] *School of Engineering, University of Aberdeen, Aberdeen, AB24 3UE, UK*
[3] *Zhejiang Province Key Laboratory of Soil Contamination Bioremediation, School of Environment and Resources, Zhejiang Agriculture and Forestry University, Hangzhou 311300, China*

ARTICLE INFO

Article history:
Received 7 February 2025
Received in revised form
29 April 2025
Accepted 7 May 2025
Available online 13 August 2025

Keywords:
Steel slag
Biomass
Hydrogen
CO_2 capture
Catalytic gasification

ABSTRACT

Conventional steam reforming for hydrogen production is limited by the thermodynamic equilibrium. To address this limitation, in this study, a cost-effective catalyst-sorbent hybrid material was synthesized from waste steel slag and limestone. A 30-cycle CO_2 sorption experiment and a sorption-enhanced biomass reforming for hydrogen production experiment were conducted. The results indicate that for the $A_4L_3S_2$ (4 mol·L^{-1} acid, limestone: slag = 3:2) composite, it attains a total CO_2 sorption capacity of 4.14 g·g^{-1} under mild conditions, with only a 23.5% reduction after 30 cycles. Moreover, under severe conditions, it manages to retain 3.81 g·g^{-1} in total 30 cycle. When applied to sorption-enhanced biomass gasification using pine wood shavings, the material significantly boosts hydrogen production, achieving a hydrogen purity of 74.57% and a yield of 0.818 mmol·g·g^{-1}·min^{-1}, while reducing the CO_2 concentration in the syngas to 10.89%. These findings highlight the dual functionality and robustness of the steel slag-derived material, offering a cost-efficient and environmentally sustainable pathway for industrial hydrogen production and valorization of solid waste resources.

1. Introduction

Since the Industrial Revolution, fossil energy has been widely used as fuel, which, although created immense wealth for humanity during certain periods, has also led to increasingly severe environmental issue. The demand for energy in human society continues to rise [1–4]. However, the formation of traditional fossil fuels is an extremely lengthy process, which undoubtedly brings potential energy crises. If this situation persists for an extended period, environmental pollution and energy crises will severely hinder the sustainable development of human society. In light of this, finding clean, efficient, and renewable energy to replace traditional fossil fuels has become key to addressing environmental pollution and energy crisis issues. Hydrogen, being widely available in elemental form in nature and featuring clean and pollution-free combustion characteristics, is regarded as an ideal energy source. It has emerged as one of the candidates most promising for replacing fossil fuels [5,6]. Moreover, hydrogen has been widely applied in many industrial production areas, such as fuel upgrading, ammonia synthesis, power generation, and fuel cells [7–11]. It occupies a crucial position in the energy sector and offers numerous advantages for future sustainable development. Currently, global demand for hydrogen is increasing year by year. It is estimated that by 2040, the annual demand for hydrogen will reach 150 million tons, equivalent to replacing the use of approximately 18 million barrels of oil [12–14]. Furthermore, the development and utilization of hydrogen energy are vital for the advancement of a low-carbon economy. For this reason, hydrogen production technology has received widespread attention in research and industry.

* Corresponding author.
E-mail address: guozhaoji@dlut.edu.cn (G. Ji).

https://doi.org/10.1016/j.cjche.2025.05.041

Currently, the methods for producing hydrogen mainly include electrolysis of saltwater, microbial fermentation, solar water splitting, biomass hydrogen production, and hydrogen production from fossil fuels [15–19]. Among these hydrogen production methods, the technology which is used to produce hydrogen from fossil fuels is the most mature one, with various processes developed, such as coal gasification, natural gas steam reforming, and thermal cracking of oil [11,20–24]. Notably, over 50% of hydrogen globally is obtained through natural gas steam reforming [24,25]; however, this industrial hydrogen production process has not eliminated dependence on traditional fossil fuels. Moreover, in the conventional steam reforming process, it is typically possible to obtain only about 70% (vol) H_2 from the reaction products, while the CO_2 concentration can exceed 20% (vol) [26]. This significantly limits the use of H_2 and leads to a series of issues, such as the greenhouse effect. Additionally, this hydrogen production process faces challenges such as high energy consumption, catalyst sintering at high temperatures, and a complex and costly separation process [27]. Therefore, it is essential to seek a new hydrogen production pathway that is clean, efficient, and economical. Biomass is considered to have broad application prospects in steam reforming for hydrogen production due to its wide availability and renewability [28,29]. Compared with traditional fossil fuels, biomass exhibits carbon neutrality during its use. Although biomass does emit CO_2 into the atmosphere during utilization, the carbon present in biomass originates entirely from atmospheric CO_2 *via* photosynthesis [30]. Besides, considering the char production after biomass gasification which fixed carbon as a stable solid, the net carbon emissions during this process could be negative.

However, the hydrogen production process through biomass steam reforming still faces the challenges inherent in conventional steam reforming technologies, leading to low hydrogen concentration and yield in the product, high separation costs, and significant energy consumption. To address these issues, researchers have explored a more economically efficient hydrogen production pathway known as 'sorption-enhanced biomass steam reforming' [31–35]. In this process, high-temperature hybrid materials are added during steam reforming [34,36,37], which *in situ* removes CO_2 produced in the reforming reaction. This disrupts the original thermochemical equilibrium, pushing the reaction toward hydrogen production, significantly increasing hydrogen concentration and yield, while also reducing the required reforming temperature. Moreover, this technology couples the reforming reaction with separation together, effectively lowering treatment costs. In sorption-enhanced biomass steam reforming, the CO_2 sorption capacity of the sorbent is closely related to the effectiveness of the reforming reaction, thereby impacting the final hydrogen concentration and output. As a result, selecting an appropriate high-temperature CO_2 sorbent is a critical factor in producing hydrogen with a high concentration. Given their high sorption capacity, Ca-based sorbents are frequently paired with transition metal catalysts like Ni and Fe to form composite functional materials. Sun *et al.* [38] studied the dual-functional catalytic performance of nickel-loaded cerium-modified CaO-based materials (Ce-CaO-Ni) and proposed an integrated method for achieving CO_2 capture and conversion in a single reactor. By adding cerium oxide (CeO_2), this material exhibited excellent cyclic stability and could maintain good performance after 20 cycles. Saupsor *et al.* [39] investigated the sorption-enhanced reforming of ethanol for hydrogen production using Fe_2O_3 as the oxygen transporter and modified CaO-Al_2O_3 as the CO_2 sorbent. The results showed that the catalyst with 5% (mass) Fe loading, prepared by the impregnation procedure, exhibited the best sorption capability at 600 °C, achieving 70% hydrogen purity in the pre-breakthrough stage and maintaining stable performance for at least five cycles. Quan *et al.* [40] studied the catalytic activity and CO_2 sorption performance of a new type of composite catalyst (Ni–Ce–Ca-ceramic membrane) in the gasification reforming of biomass (pine sawdust). Its optimal performance is as follows: the lowest CO_2 content in the gasification gas production is 8.18% (vol), the CO_2 production rate is 2.1 $mmol \cdot g^{-1}$, and the hydrogen production rate reaches up to 14.19 $mmol \cdot g^{-1}$. After deactivation, a new batch of fresh functional material must be fed to replace the old batch, and this process requires a large amount of material. Most of the existing research about catalyst-sorbent hybrid material used commercial chemicals as material sources, making the material cost unfavorable economically. If the hybrid functional material is from abundant solid wastes, the expense of the material would be substantially reduced.

Steel slag is a by-product or waste of the steel production process, and it contains all the necessary components for a catalyst-sorbent hybrid functional material such as CaO (20% to 50%) for sorption, Fe_2O_3 (15% to 35%) and MnO (1% to 5%) for reforming catalysis, and Al_2O_3 (2% to 8%), SiO_2 (8% to 20%), MgO (4% to 13%) for stabilization. In the steel production process, approximately 130 kg of steel slag are produced for every ton of crude steel produced. According to data from the China Association for Recycling and Utilization of Steel Slag, China's steel slag production reached 121 million tons in 2018. From the early 1990s to the end of 2018, China's cumulative storage volume of steel slag exceeded 1.8 billion tons, occupying an area of over 200000 Chinese mu (1 mu $\approx$ 666.67 m^2). In 2018, China's crude steel output was 9.28 billion tons, accounting for about half of global crude steel output. Wang *et al.* [41] synthesized a CaO-based CO_2 sorbent using steel slag. The sorbent shows good sorption performance and maintains remarkable stability over multiple cycles. The results showed that the sorption capacity can reach 81% of the theoretical sorption capacity of CaO. After 30 cycles, it still maintained a stability that was higher than that of commercial $Ca(OH)_2$. Tian *et al.* [42] converted steel slag as the only raw material into a superior CaO-based self-stabilizing CO_2 sorbent. The CO_2 capture capacity of the sorbent after acetic acid treatment is over 10 times than original steel slag. After 30 carbonation-calcination cycles, the decay rate was only 12%, and the maximum uptake of CO_2 reached 0.50 $g \cdot g^{-1}$. Zhang *et al.* [43] prepared steel slag-derived CaO. After 35 sorption/desorption cycles, this CaO exhibits a good CO_2 capture performance with stability of approximately 0.48 $g \cdot g^{-1}$. It is analyzed that the main reasons for this are the mesoporous structure as well as the presence of Fe_2O_3. Modifying steel slag to prepare Ca-based sorbents as substitutes for sorbents can reduce the consumption of natural resources and enhance the resource utilization efficiency of steel slag. In addition, the deactivated sorbents after the reaction can be directly recycled as raw materials into blast furnaces or converters for steelmaking [44], thus achieving the goal of the coordinated development of waste resource utilization and waste recycling.

Existing research had demonstrated the feasibility of steel slag-derived material as high-temperature CO_2 sorbent. Since it also contains transition metal oxides, it also has great catalytic potential to be used as hybrid functional material for biomass gasification [45]. Moreover, the inherent elements such as Al_2O_3 and SiO_2 might form rigid stabilizer to enhance the anti-sintering effect of the functional material, this could reduce the frequency of refreshing the deactivated functional material, further reducing the material cost. This study would utilize steel slag as the source material to synthesize catalyst-sorbent hybrid functional material, test its CO_2 sorption performance at gasification temperatures and assess its capability in enhancing hydrogen production from biomass waste gasification in a tube reactor. This study could pave

the road of using slag solid waste to promote valuable hydrogen production from biomass wastes.

2. Experimental

2.1. Steel slag-derived hybrid material preparation

The steel slag and limestone used in this experiment were sourced from Anshan Iron and Steel Group Corporation, China. The elemental composition of the steel slag and limestone, was determined by using X-ray fluorescence spectroscopy (XRF, Axios, PANalytical, USA) and expressed in the form of oxides, shown in Table 1. Other component includes titanium oxide (TiO_2), sulfides (such as CaS, MnS), phosphides (such as P_2O_5), and dicalcium silicate ($2CaO \cdot SiO_2$, C_2S), *etc.*

Table 2 shows the synthesis parameters of nine steel slag-based composite materials. The predetermined amounts of steel slag and limestone were mixed with a certain concentration of acetic acid solution at a solid (g)-liquid (l) ratio of 1:30. After that, the mixture underwent mechanical treatment and was stirred at room temperature at a rotation speed of 500 $r \cdot min^{-1}$. After 45 min, the stirring was stopped, and the mixture was centrifuged to obtain the steel slag leachate and the centrifugal precipitation phase (*i.e.*, the acid-leaching residue). The leachate from steel slag which was obtained was dried at 105 °C for 12 h to obtain the fresh steel slag-derived hybrid material. Then, the dried sample was calcined in an air at 900 °C for 2 h to finally obtain the stabilized steel slag-derived hybrid materials as shown in Fig. 1. The hybrid material was named as $A_XL_YS_Z$, where *X* represents the initial acid concentration, and *Y* and *Z* represent the mass ratio of limestone to steel slag. Taking $A_2L_4S_1$ as an example, A_2 indicates that the initial acid concentration for the preparation of this hybrid material is 2 $mol \cdot L^{-1}$, and L_4S_1 indicates that this hybrid material was fabricated through the combination of limestone and steel slag at a ratio of 4:1. The CO_2 sorption and hydrogen production performance of the newly synthesized sorbents was evaluated by taking commercially available calcium oxide (CaO) as a benchmark.

2.2. Characterization of steel slag-derived hybrid material

The main elemental composition of steel slag-derived hybrid material was determined by X-ray fluorescence spectrometer (XRF, Axios, PANalytical, USA). This is to determine the elemental compositions of various steel slag-based composite materials so as to facilitate the subsequent analysis of the relationship between performance and elemental proportions.

The phase composition and crystal phase structure were tested by X-ray diffractometer (XRD, D8 Advance, Bruker Corporation, Germany) using Cu K_α (40 kA, 100 mA) radiation, scanning rate of 8 $(°) \cdot min^{-1}$ and sample scanning range (2θ) from 10° to 90°. The grain size of CaO at 37° (200) crystal plane was calculated by the Scherrer equation (results in Table 3). The XRD test is used to determine the phases formed in the composite materials, calculate the grain size of CaO. These information could ascertain whether the steel slag has effectively participated in the reaction, and determine how different preparation methods affect the composite materials.

Table 1
The elemental composition of steel slag and limestone raw materials (%, mass).

Sample	Composition						
	CaO	Fe_2O_3	SiO_2	Al_2O_3	MgO	MnO	Others
Steel	14.38	38.16	24.18	4.52	3.16	2.84	12.76
Limits of error	±8.31	±3.73	±7.36	±3.16	±1.82	±0.52	±2.37
Limestone	87.54	0.71	4.21	0.41	6.39	0.16	0.58
Limits of error	±4.32	±0.17	±1.36	±0.28	±1.03	±0.27	±0.16

The NOVA NanoSEM 450 field emission scanning electron microscope by FEI Company (USA) was used to observe the microscopic surface morphologies of fresh and used steel slag-derived hybrid material. Meanwhile, an X-ray energy dispersive spectrometer-Mapping (EDS-Mapping) was used to analyze material elements simultaneously to explore the relationship between microscopic surface morphologies and hybrid material performance. As the electrical conductivity is poor, the samples were coated with gold by sputtering before observation. This step involves analyzing the relationship between the performance of the composite materials, the differences in their microscopic morphologies and the uniformity of element distribution.

The AS-1-MP-11 fully automatic physical sorption instrument by Quantachrome Instruments (USA) was used to conduct N_2 physical sorption tests on steel slag-derived hybrid material. The specific surface area, pore size and pore volume arrangement of synthesized materials were determined by BET surface area analysis and BJH pore size distribution. Before the N_2 sorption test, samples were degassed at 300 °C for at least 3 h to remove water and other gaseous impurities sorbed during preparation and storage. The BET test is mainly aimed at quantifying the textual property, such as surface area, pore volume, pore size and size distribution.

2.3. Cycle CO_2 capture experiment

The thermogravimetric analyzer (TGA, Netzsch STA449F5, Germany) was employed to evaluate the CO_2 sorption capacity and cyclic stability of steel slag-derived hybrid material under mild and severe conditions. To facilitate the comparison and evaluation of the performance of different sorbents, a commonly used standard test condition was selected: For the mild test condition, a sample weighing (5 ± 1) mg was positioned in a quartz crucible. Subsequently, the sample was heated to the calcination temperature of 850 °C in a pure nitrogen atmosphere and held for 10 min to remove impurities formed during storage. After calcination, the temperature was chilled to the carbonation temperature of 650 °C in a pure nitrogen atmosphere. Once the temperature reached 650 °C, the gas was switched to 15% (vol) CO_2 (balanced with N_2) and maintained for 30 min. After the carbonation reaction, the sample was heated back to the calcination temperature of 850 °C in pure nitrogen and held for 30 s. Then, the next cycle commenced. The total gas flow rate was fixed at 100 $ml \cdot min^{-1}$, with heating and cooling rates controlled at 20 $°C \cdot min^{-1}$ during the experiment.

Under the severe conditions, after the first calcination process, the sample was cooled to the carbonation temperature of 650 °C at a speed of 20 $°C \cdot min^{-1}$ in a pure nitrogen atmosphere. As soon as the temperature reached 650 °C, the atmosphere was changed to 15% (vol) CO_2 (balanced with N_2) and maintained for 5 min. After the carbonation reaction, the sample was heated to 950 °C at 30 $°C \cdot min^{-1}$ in an atmosphere of 90% (vol) CO_2 (balanced with N_2) and calcined for 30 s before starting the next cycle. In the course of the experiment, the total gas flow rate was also kept at 100 $ml \cdot min^{-1}$.

The CO_2 sorption performance of steel slag-derived hybrid material is assessed by the following five defined indicators: (1) CO_2 sorption capacity (the mass of CO_2 sorbed per unit mass of hybrid material, denoted as C_i, in units of $g \cdot g^{-1}$); (2) CaO conversion rate (the percentage of the CaO active component in the hybrid material that is carbonated, represented as X_i, %); (3) total CO_2 sorption amount in 30 cycles (the total amount of CO_2 sorbed

Table 2
Synthesis parameters of nine steel slag-derived hybrid material.

Sample	Factor					
	Limestone/g	Steel slag/g	Concentration of acetic acid/mol·L^{-1}	Ratio of solid to liquid/ml·g^{-1}	Temperature/°C	Time of acid leaching/min
$A_2L_4S_1$	4	1	2	1:30	45	45
$A_2L_3S_2$	3	2	2	1:30	45	45
$A_2L_1S_4$	1	4	2	1:30	45	45
$A_4L_4S_1$	4	1	4	1:30	45	45
$A_4L_3S_2$	3	2	4	1:30	45	45
$A_4L_1S_4$	1	4	4	1:30	45	45
$A_6L_4S_1$	4	1	6	1:30	45	45
$A_6L_3S_2$	3	2	6	1:30	45	45
$A_6L_1S_4$	1	4	6	1:30	45	45

by unit mass of hybrid material within 30 cycles, designated as C_T, in units of g·g^{-1}); (4) average deactivation rate per cycle (κ_{DR}, in units of g·g^{-1}); (5) theoretical cycle number (N_{thr}, in cycles).

$$C_i = \frac{m_{max,i} - m_{min,i}}{m_0} \quad (1)$$

$$X_i = \frac{C_i \times M_{CaO}}{\eta \times M_{CO_2}} \times 100\% \quad (2)$$

$$C_T = \sum_{i=1}^{30} C_i \quad (3)$$

$$\kappa_{DR} = \frac{C_{max,n'} - C_{30}}{30 - n'} \quad (4)$$

$$N_{thr} = \frac{C_{max,n'}}{DR} \quad (5)$$

In Eqs. (1)–(5), $m_{max,i}$ denotes the mass of the hybrid material subsequent to the ith cyclic carbonation reaction, and $m_{min,i}$ denotes the mass of the hybrid material prior to the ith cyclic carbonation reaction. m_0 is the initial mass of the hybrid material. The molar masses of CaO and CO_2 are denoted by M_{CaO} and M_{CO2} respectively. η indicates the mass fraction of CaO in the hybrid material. Shows the maximum sorption capacity of CO_2 within 30 cycles, with n' being the corresponding cycle number. A lower κ_{DR} value combined with a higher N_{thr} value implies superior anti-sintering performance of the hybrid material

2.4. Hydrogen production experiment

Sorption-enhanced hydrogen production experiments were carried out in a downstream quartz tube fixed-bed reactor (24 mm inner diameter, 1000 mm long), which is shown schematically in Fig. 2. The setup can be divided into six main parts: gas feeding system, the steam feed system, reaction system, cooling device and product collection system. The gas feeding system is made up of a high-pressure cylinder and a gas mass flow controller; the steam feed system consists of a single-channel micro syringe pump and a preheater; the reaction system includes a two-end high-temperature resistance furnace, a temperature controller and a quartz tube with a pusher at the top and a mesh in the middle; the cooling device consists of a condensation tube and a low-temperature coolant circulating pump; the product collection system collects the syngas through a gas bag, and gas products were analyzed using gas chromatography (GC). In order to further analyze the roles of various components, a blank group, a steel slag group, a commercial CaO group, and an Fe_2O_3 group were set up as controls. The gasification temperature and the reaction temperature are selected to be 600 °C [46]. The specific operation steps of the experiment are as follows:

(a) Firstly, place 0.5 g of pine wood shaving in the iron mesh at the bottom of the push rod and position the push rod at the

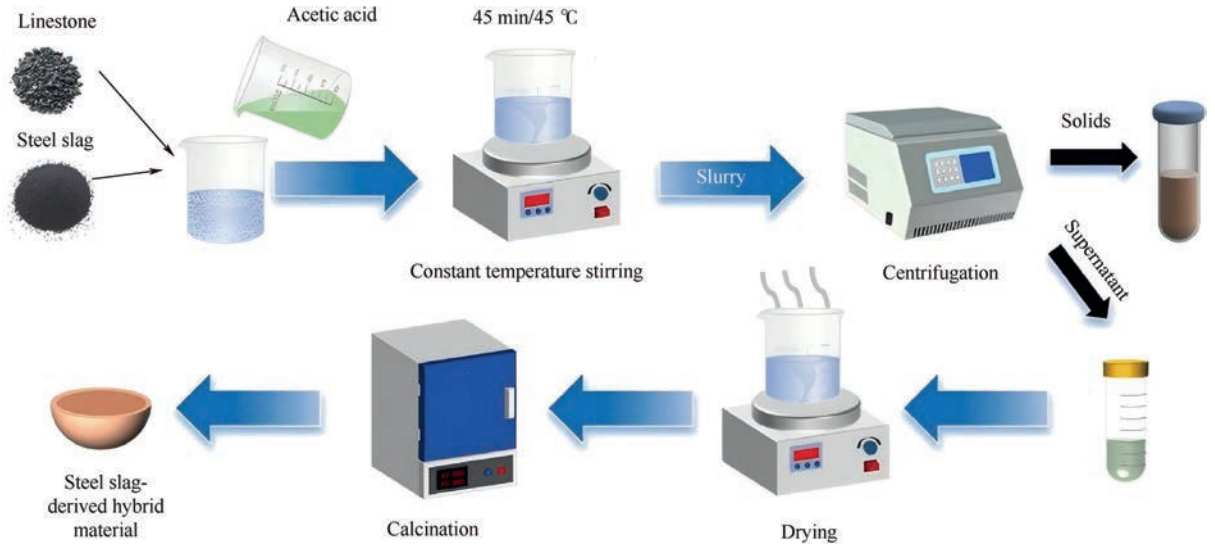

Fig. 1. Flowchart of sample preparation.

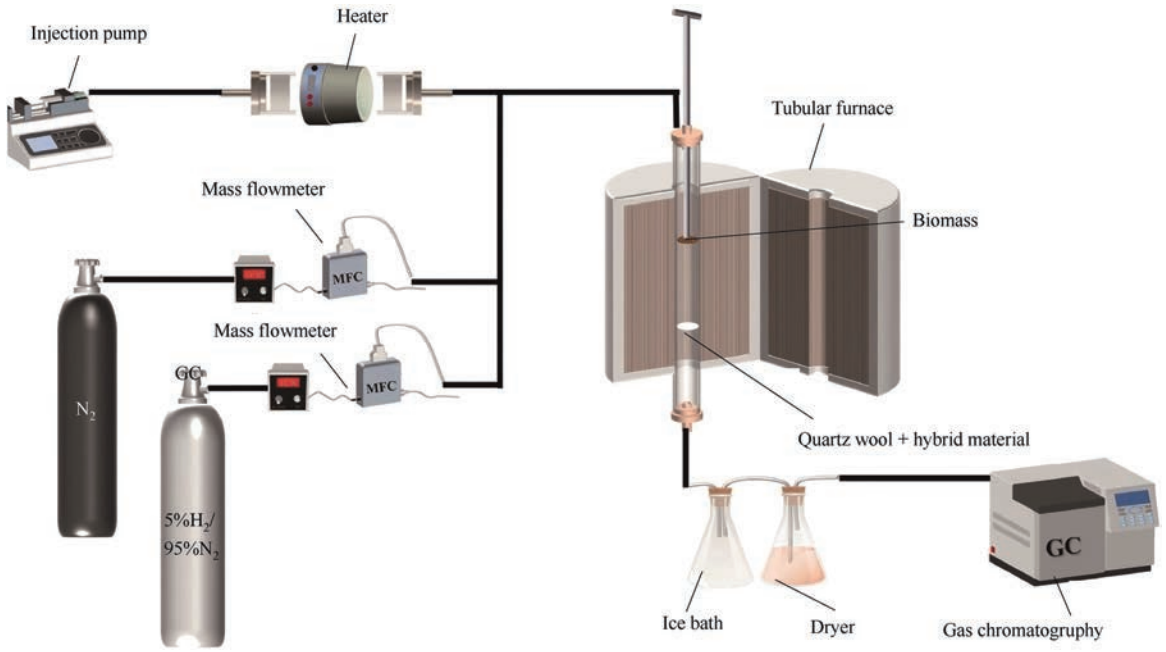

Fig. 2. Experimental device for enhancing hydrogen production from biomass steam reforming.

uppermost end. Place 0.5 g hybrid material on the quartz wool at the bottom. Then, lay a layer of quartz wool on top of the catalyst.

(b) Secondly, introduce nitrogen (N_2) at a flow rate of 100 ml·min^{-1}. The lower portion of the reactor is heated from room temperature up to 850 °C at a rate of 20 °C per minute, and maintain this temperature for 30 min to remove the impurities generated during the preparation and storage of the integrated material. After the calcination was completed, the type of gas was switched to 5% H_2/95% N_2, flowing at a rate of 100 ml·min^{-1}. Then, the catalyst was reduced at 700 °C for 30 min to ensure that all catalytic components were reduced to metal states. Then, cool it down to 600 °C.

(c) Start heating the upper part of the reactor until it reaches 600 °C. Then, turn on the micro-injection pump to vaporize pure water with a 1:1 steam-to-biomass (S/B, ml·g^{-1}) ratio through a preheater at 180 °C and introduce it into the reactor at a certain feed rate. Push the push rod to the center position of the upper furnace. The reaction time is 10 min. After passing through the condensation system and drying system at the outlet of the reactor, the products are collected in gas bags.

(d) After the gas collection is completed, use a gas chromatograph (8860GC, Agilent, USA) to analyze the products in the gas bags.

The gaseous products from sorption-enhanced biomass steam reforming for hydrogen production were detected by gas chromatography, and the products were sufficiently dominated by CH_4, CO_2, CO, and H_2, and the various gaseous components in the products were quantitatively analyzed by the volume concentration normalization method. In the biomass steam reforming process enhanced by sorption, the concentration of each component and the H_2 yield were calculated by the following formula. The concentration which pertains to each gas component (P_i):

$$P_i = \frac{C_i}{C_{H_2} + C_{CO_2} + C_{CO} + C_{CH_4}} \times 100\% \quad (6)$$

where i represents the four gas components CH_4, CO_2, CO and H_2 and C_i denotes the volume concentration of each gas component in the gas product.

In pine wood shaving gasification, following chemical reactions take place.

Boudouard reaction:

$$C + CO_2 \rightleftharpoons 2CO \quad (7)$$

Water–gas reaction:

$$C + H_2O \rightleftharpoons CO + H_2 \quad (8)$$

Methanation:

$$C + 2H_2 \rightleftharpoons CH_4 \quad (9)$$

Water-gas shift reaction (WGS):

$$CO + H_2O \rightleftharpoons CO_2 + H_2 \quad (10)$$

Steam-methane-reforming reaction:

$$CH_4 + H_2O \rightleftharpoons CO + 3H_2 \quad (11)$$

Sorption reaction:

$$CaO + CO_2 \rightleftharpoons CaCO_3 \quad (12)$$

3. Results and Discussion

3.1. Characteristics of main elements in the steel slag-derived hybrid material

Table 4 shows the composition of the nine prepared steel slag-derived hybrid material. Since calcium oxide is the main component of CO_2 sorption, the fraction of CaO has an important

influence on the capability of hybrid materials. The effect of mixing ratio on the CaO fraction is extremely obvious, with the increase of steel slag, the CaO fraction decreases significantly, and the fraction of Fe_2O_3, Al_2O_3 and SiO_2 increased significantly. There are some inert metal oxides (such as Al_2O_3) in hybrid material. Following calcination, they can supply a supporting structure to stop the deactivation of active component CaO and significantly improve the cycle stability of the sorbent [47]. The CaO content of the six samples with doping ratios of 4:1 and 3:2 in the prepared hybrid materials is higher than 50%, and the highest content of the three hybrid materials of L_1S_4 series is only 35.67%. The initial acid concentration has little effect on the hybrid material composition. High concentration of acid can leach more Ca, but the other metal elements in steel slag will also be leached, which leads to the insignificant change of overall percentage of Ca. In addition to the Ca element, the elements that are significantly affected by the initial acid concentration are Fe and Si. The content of Fe element in the samples of A_4 series and A_6 series is not very different, but both are much higher than the samples of A_2 series.

As the concentration of acetic acid solution increases, the H^+ concentration also increases accordingly, which simultaneously increased the limestone and steel slag solubility in the liquid phase. Despite the increase in calcium leaching, the simultaneous increase in the leaching of other elements from the steel slag resulted in an insignificant increase in the calcium content of the hybrid material. In conclusion, a high acid concentration has a relatively limited influence on the sorption capacity and will additionally increase costs. On the other hand, an excessively low acid concentration will lead to a decrease in production yield. Therefore, it is of great significance to further explore how to control the acid concentration and doping ratio properly to ensure that the composite material can maintain a high calcium content while also possessing a sufficiently high proportion of inert components.

3.2. The CO_2 sorption performance of steel slag-derived hybrid materials

Under mild testing circumstances, the influences of various doping ratios on the cyclic CO_2 sorption capability and the conversion rate of CaO in steel slag-derived hybrid materials were explored. The outcomes are presented in Fig. 3. The CO_2 sorption capacity of commercially available CaO rapidly dropped from 0.293 $g \cdot g^{-1}$ in the initial cycle to 0.078 $g \cdot g^{-1}$ after the 30th cycle. This corresponds to a reduction in CaO conversion from 66.65% to 17.62%. The agglomeration and sintering of CaO particles during high-temperature calcination lead to this decline, resulting in substantial pore collapse and a loss of specific surface area. Compared to commercial calcium oxide, the CO_2 sorption capacity of the steel slag-based composite (mixed) material did not show a significant advantage during the initial cycle phase. However, the hybrid materials maintained a relatively high sorption capacity over multiple cycles, demonstrating improved cyclic stability. With an increase in steel slag content, the stability of the hybrid material exhibited an increasing trend, following the order of L_4S_1 series > L_3S_2 series > L_1S_4 series. Among these, $A_2L_4S_1$ demonstrated the highest total sorption capacity over 30 cycles. Nevertheless, it experienced rapid deactivation within the first 10 cycles, with the CaO conversion rate declining from 58.91% in the initial cycle to 43% after the 10th cycle. This behavior was attributed to the insufficient steel slag content to stabilize the skeletal structure of CaO. After 30 cycles, the L_1S_4 series sorbent exhibited the best anti-sintering performance but the lowest CO_2 sorption capacity. For example, $A_6L_1S_4$ retained approximately 0.020 $g \cdot g^{-1}$ loss in capacity after 30 cycles and achieved a 72.78% CaO conversion rate. This enhanced performance was attributed to the higher steel slag content, which improved sintering resistance and suppressed the agglomeration of CaO particles. The addition of higher steel slag contents provided structural stability, thereby inhibiting CaO sintering. The insets in Fig. 3 illustrate the total CO_2 sorption capacity per gram of steel slag-derived hybrid material over 30 cycles. The hybrid materials followed the descending order: $A_2L_4S_1 > A_4L_3S_2 > A_4L_4S_1 > A_6L_4S_1 > A_2L_3S_2 > A_6L_3S_2 > CaO > A_2L_1S_4 > A_4L_1S_4 > A_6L_1S_4$. Notably, blending with a high content of steel slag significantly enhanced the cyclic durability of the hybrid material. However, this improvement was accompanied by a reduction in CaO content, which limited the theoretical CO_2 sorption capacity of the material. Conversely, in the absence of or with minimal incorporation of steel slag, while the theoretical CO_2 sorption capacity is retained, the resistance to sintering of the CaO-based hybrid material is attenuated. Consequently, the CO_2 sorption capacity undergoes a swift decline as the cycles progress. This trade-off explains why materials like $A_4L_4S_1$, $A_6L_4S_1$, and commercial CaO, which have a higher CaO content, fail to achieve the desired cumulative CO_2 sorption capacity over multiple cycles. In contrast, $A_2L_4S_1$, with its highest theoretical CO_2 sorption capacity (0.639 $g \cdot g^{-1}$) among the nine hybrid materials, sorbed the largest amount of CO_2 (4.43 $g \cdot g^{-1}$) over 30 cycles. Additionally, $A_4L_3S_2$ achieved the second-highest total CO_2 sorption capacity (4.14 $g \cdot g^{-1}$), attributed to its balanced elemental distribution, which conferred both high sorption capacity and stability.

Table 3
The BET surface area, BJH pore volume and CaO grain size of steel slag derived hybrid material.

Sample	Fresh			Used		
	BET surface area /$m^2 \cdot g^{-1}$	Pore volume /$cm^3 \cdot g^{-1}$	Crystalline size of CaO /nm	BET surface area /$m^2 \cdot g^{-1}$	Pore volume /$cm^3 \cdot g^{-1}$	Crystalline size of CaO /nm
$A_2L_4S_1$	9.1	0.054	47.3	3.2	0.019	>100
$A_2L_3S_2$	6.3	0.039	63.1	3.4	0.021	>100
$A_2L_1S_4$	3.8	0.031	75.8	2.4	0.020	>100
$A_4L_4S_1$	9.8	0.058	53.8	3.7	0.022	>100
$A_4L_3S_2$	9.2	0.050	65.3	5.2	0.036	>100
$A_4L_1S_4$	4.2	0.038	83.1	2.7	0.024	>100
$A_6L_4S_1$	11.5	0.105	59.6	5.5	0.050	>100
$A_6L_3S_2$	10.1	0.093	75.0	4.9	0.045	>100
$A_6L_1S_4$	4.8	0.051	90.7	3.3	0.035	>100

For a more comprehensive evaluation of the cyclic CO_2 sorption performance exhibited by the steel slag-derived hybrid materials, the average deactivation rate (κ_{DR}) and the theoretical number of cycles (N_{thr}) were computed. The corresponding results are depicted in Fig. 4. Commercial CaO demonstrated the highest κ_{DR} (0.0072) and the lowest N_{thr} (40.78), mainly due to sintering effects. The average deactivation rate of the hybrid materials decreased with increasing steel slag content, which was attributed to enhanced physical segregation that effectively inhibited sintering [48]. Among the hybrid materials, those synthesized with an initial acid concentration of A_6 demonstrated lower κ_{DR} and higher N_{thr} values compared to the A_2 and A_4 series, indicating superior stability over 30 cycles. Notably, $A_4L_3S_2$ displayed significant advantages in both κ_{DR} and N_{thr} values among the hybrid materials with the same doping ratios, further confirming its excellent sorption performance. In conclusion, higher doping ratios and acid concentrations significantly increased the inert metal fraction in the hybrid materials. Among these factors, the influence of doping ratios was particularly pronounced, contributing to the improved stability of the steel slag-derived hybrid materials. This conclusion aligns with the compositional analysis of the steel slag-derived materials. As shown in Fig. 4, $A_2L_4S_1$ and $A_4L_3S_2$ were identified as the preferred hybrid materials for subsequent tests under

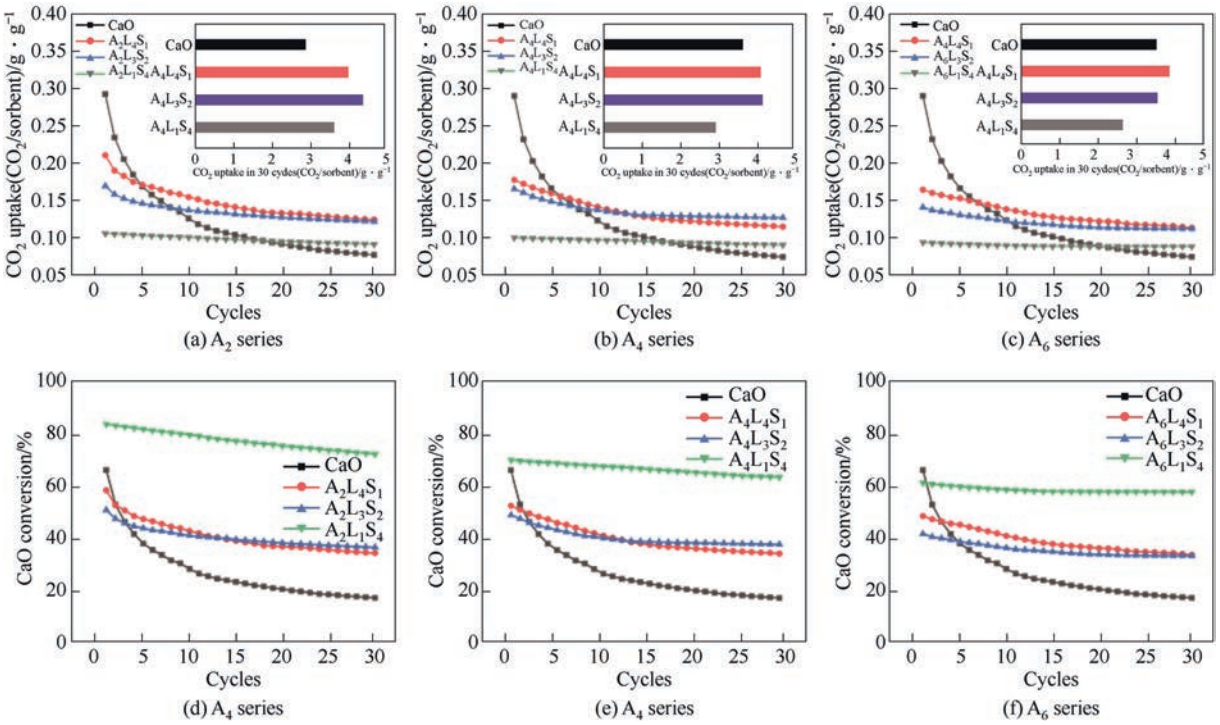

Fig. 3. CO_2 capture capability of commercial CaO and prepared nine steel slag-derived hybrid materials over 30 cycles under mild conditions: 15% CO_2/85% N_2 at a temperature of 650 °C lasting for 5 min; calcination: 100% N_2 with 850 °C for 30 s). A_2 Series (a) and (d), A_4 Series (b) and (e) and A_6 Series (c) and (f).

severe sorption conditions and biomass reforming experiments, due to their outstanding behavior in the 30-cycle tests.

The 30-cycle CO_2 capture behavior of the high-performance hybrid materials ($A_2L_4S_1$ and $A_4L_3S_2$), along with the hybrid material exhibiting the best stability ($A_6L_1S_4$), was studied under stringent test conditions. These test conditions involved regenerating the used materials through calcination at high temperatures under CO_2-rich conditions. As illustrated in Fig. 5, given that the carbonation and initial calcination conditions under severe circumstances were equivalent to those in mild settings, the hybrid materials exhibited nearly the same CO_2 sorption capacity during the first cycle as that witnessed under milder conditions.

However, the first carbonation reaction CO_2 sorption capacity of the selected preferred hybrid materials declined rapidly from the second cycle due to the harsh calcination conditions, characterized by a higher CO_2 concentration of 90 vol% and elevated temperature (950 °C). As depicted in Fig. 5(a), the sorption capacity of CO_2 for commercial CaO dropped significantly from 0.264 $g \cdot g^{-1}$ in the first cycle to 0.0683 $g \cdot g^{-1}$ by the 30th cycle. In comparison with milder conditions, the accelerated deactivation witnessed under severe conditions was predominantly ascribed to the intensified sintering and agglomeration of CaO particles. In contrast, the hybrid materials, doped with steel slag, exhibited a marked improvement in their resistance to deactivation under the severe conditions. Among them, $A_4L_3S_2$ demonstrated the best resistance to sintering, retaining the highest CO_2 sorption capacity (0.114 $g \cdot g^{-1}$) during the 30th cycle, which was attributed to its superior stability. The materials' total CO_2 capture amount over 30 cycles exhibited a descending order.: $A_4L_3S_2$ > $A_2L_4S_1$ > CaO > $A_6L_1S_4$. Notably, $A_4L_3S_2$ demonstrated the most superior overall sorption capacity and durability under severe conditions over 30 cycles (3.81 $g \cdot g^{-1}$), which was likely due to its optimized CaO content and material composition. Considering both the total amount of CO_2 captured and cyclic stability, among the materials examined over 30 cycles under severe conditions, $A_4L_3S_2$ showed the optimal CO_2 capture performance.

3.3. The sorption kinetic analysis of steel slag-derived hybrid materials

An optimal CaO-based sorbent should own a fast CO_2 sorption rate in addition to having a good CO_2 sorption performance and outstanding stability during cycling. Since the CaO's CO_2 sorption capacity is mainly attained during the quick reaction stage, it is more appropriate to concentrate on the rate of CO_2 sorption at this stage. Figs. 6 and 7 present the CO_2 uptake and sorption rate versus time for both commercial CaO and steel slag-derived hybrid materials, comparing the results from the first and final cycles under mild conditions. The sorption rate was determined by monitoring the mass change of the sorbent using thermogravimetric analysis (TGA). The mass variation of the sorbent was recorded as a function of time (t), and the sorption rate was calculated by taking the first derivative of the mass change with respect to time (dm/dt). This approach provides a direct and quantitative measure of the sorption kinetics, allowing for the evaluation of the sorbent's performance under specific conditions.

The carbonation of CaO occurs in two clearly distinguishable stages: a rapid reaction phase occurring in the first minute. The reaction is characterized in such a way that there is a high reaction rate first, and Then a slower phase with a much lower rate follows, which is governed by the diffusion of CO_2 through the layer of calcium carbonate product. The nine steel slag-derived hybrid materials all exhibited higher sorption rates than that of the commercial CaO. The peak sorption rate of the CO_2 hybrid materials appeared significantly earlier (~0.75 min) than that of the commercial CaO (~1.0 min), and this rapid sorption capability is

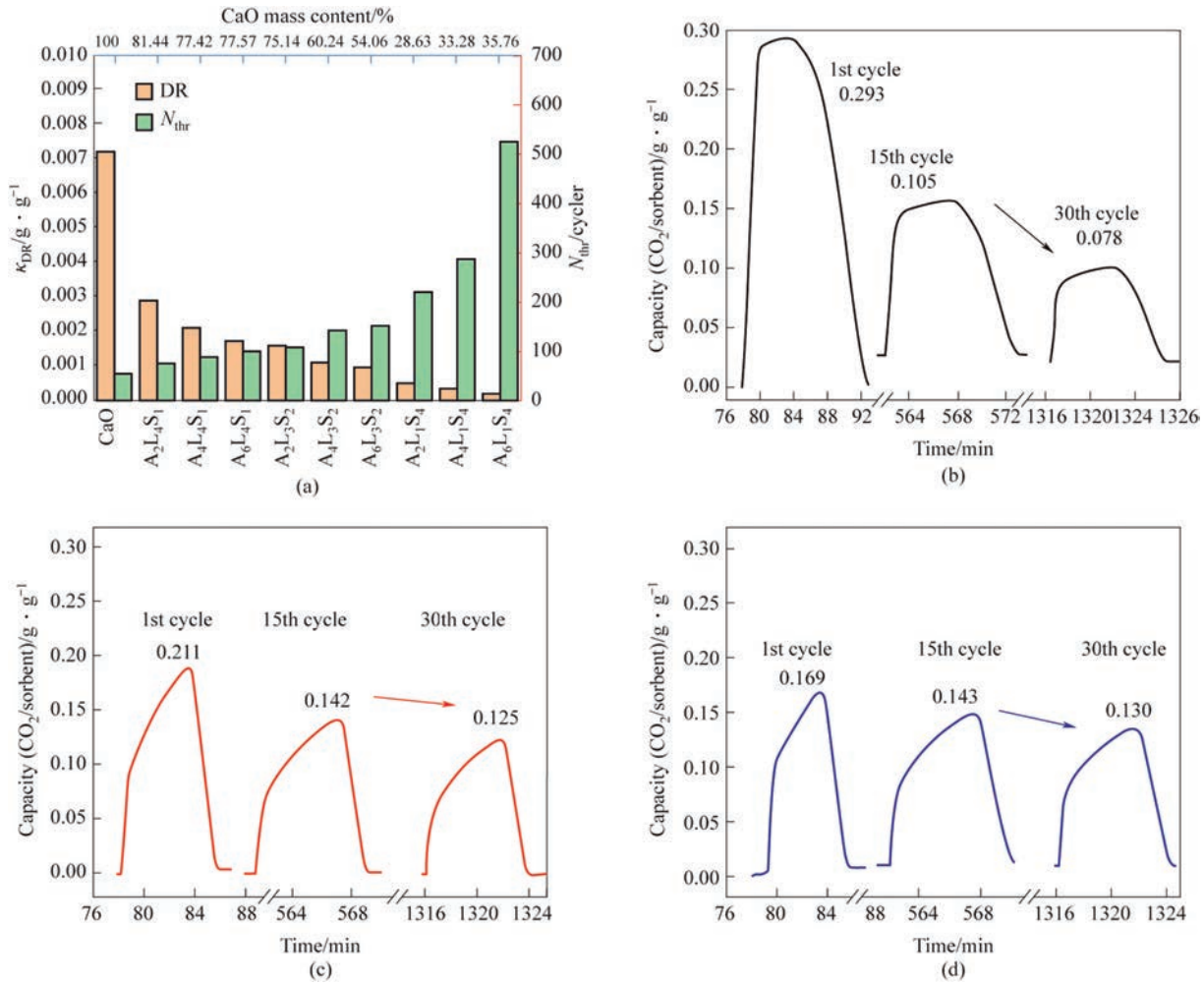

Fig. 4. Comparison of deactivation rates and theoretical cycle numbers between commercial CaO and steel slag-derived hybrid materials: (a) deactivation rates and theoretical cycle numbers of commercial CaO and steel slag-derived hybrid materials; (b), (c), and (d) CO_2 sorption performance over 30 cycles for three types of hybrid materials: CaO, $A_2L_4S_1$, and $A_4L_3S_2$, respectively.

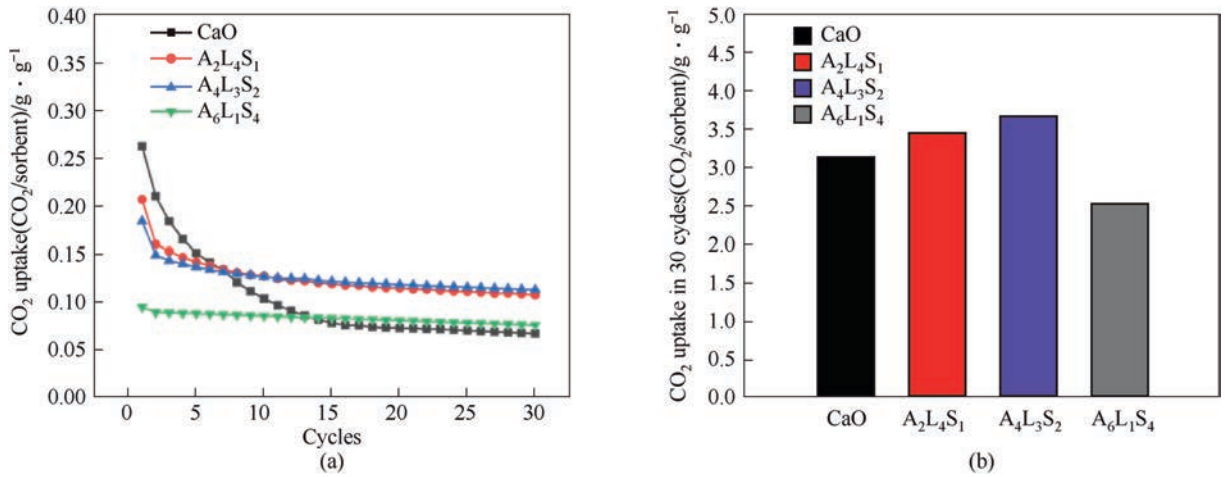

Fig. 5. The selected hybrid materials under severe conditions, the CO_2 uptake (a) and the total CO_2 uptake within 30 cycles (b).

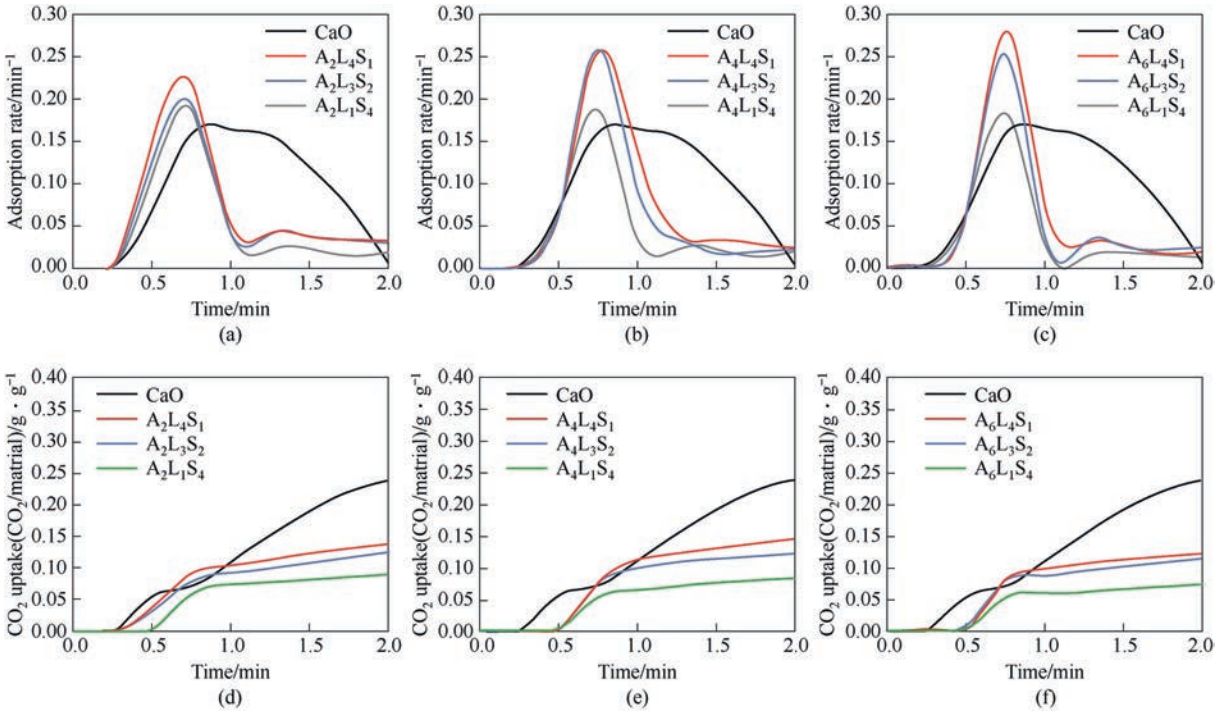

Fig. 6. Under mild conditions, carbonation kinetics of commercial CaO and nine steel slag-derived hybrid materials during the first cycle: (a), (b), and (c) CO_2 sorption rate of the nine hybrid materials in the first 2 min, respectively; (d), (e), and (f) CO_2 sorption capacities of the nine hybrid materials in the first 2 min, respectively.

more favorable for its use in fluidized bed reactors with reduced residence times. Meanwhile, after acid leaching, more pores and CO_2 sorption sites appeared in the hybrid material, both of which were more favorable for the rapid reaction between CaO and CO_2. In the first cycle, CO_2 sorption rate showed the following trends: under the condition of constant initial acid concentration: L_4S_1 Series > L_3S_2 Series > L_1S_4 Series; under the condition of constant doping ratio: A_6 Series > A_4 Series > A_2 Series. The influence of doping ratio on the sorption rate was more pronounced.

The sorption rate of commercial CaO dropped markedly in the final cycle, showing a 17.5% decrease in the peak sorption rate after 30 cycles. The severe agglomeration of CaO particles in commercial CaO after multiple cycles can be the reason for this (Fig. 7), and the nine steel slag-derived hybrid materials showed more obvious advantages, with excellent anti-sintering properties to ensure their sorption rates. Among them, the peak sorption rate of $A_6L_1S_4$ hybrid material only decreased by 13% between the first and the last cycle, which was attributed to the excellent sintering inhibition ability.

3.4. Analysis on the properties and structure-activity relationship of hybrid materials

3.4.1. XRD analysis

Fig. 8 is the XRD analysis of the nine fresh steel slag-derived hybrid materials. The main physical phase is CaO. The presence of calcium hydroxide components is mainly because the moisture in the air converted CaO to calcium hydroxide during storage. The main factor affecting the physical phase was the acid concentration. The main inert components of the six hybrid materials prepared under the conditions of A_2 and A_4 were Fe_2O_3 and to a lesser extent $Ca_2Fe_2O_5$, and the Tammann temperatures (the temperature at which atoms move) of these two components (Fe_2O_3-919 °C [49], $Ca_2Fe_2O_5$-912 °C [39]), were higher than those of $CaCO_3$ and the carbonation/calcination temperature. $Ca_2Fe_2O_5$ has been extensively reported in the literature as an effective stabilizer [50,51]. Its structure, characterized by a high concentration of oxygen vacancies, significantly reduces the diffusion resistance of O^{2-} ions [39]. This property facilitates the diffusion of O^{2-} both on the surface and within the bulk of the material. During the CO_2 absorption process, O^{2-} ions react with CO_2 to form an intermediate product, CO_3^{2-}. The existence of oxygen vacancies promotes this reaction, thereby promoting the absorption of CO_2. Notably, under typical reaction temperatures used for enhanced biomass reforming to produce hydrogen (*e.g.*, 600 °C), $Ca_2Fe_2O_5$ remains stable and continues to play a catalytic role in promoting the conversion of CO.

The three catalysts with an initial acid concentration of 6 mol·L^{-1} were different. The main inert components became $CaSi_2O_5$ (929 °C) and Ca_2FeAlO_5 (~900 °C) [52]. It has been demonstrated that those (which refer to certain materials or substances in context) with higher Tammann temperature enhance the sintering resistance of calcium-cycled materials at high temperatures. As shown in Table 3, the grain sizes of CaO at the (2 0 0) phase was determined using Scherrer's equation. After doping steel slag and acid treatment, the grain size of CaO decreases rapidly and shows a tendency to decrease with the increase of the initial acid concentration, and increase with the increase of the proportion of steel slag doping. This is because the inert component, with a high Tammann temperature, introduced by doping is uniformly dispersed within the CaO particles, forming a physical barrier to effectively prevent their growth between the CaO grains. The smaller CaO grain size enhances the exposure of active sites, thereby improving the carbonation conversion. Although other elements (*e.g.*, Al, Mg, Mn, *etc.*) were present in the XRF analysis, the samples contained more iron and less other elements, which were not obviously detected in the XRD analysis.

3.4.2. BET analysis

The nine steel slag-derived hybrid materials were tested for N_2 physical sorption and desorption. As for the specific surface area

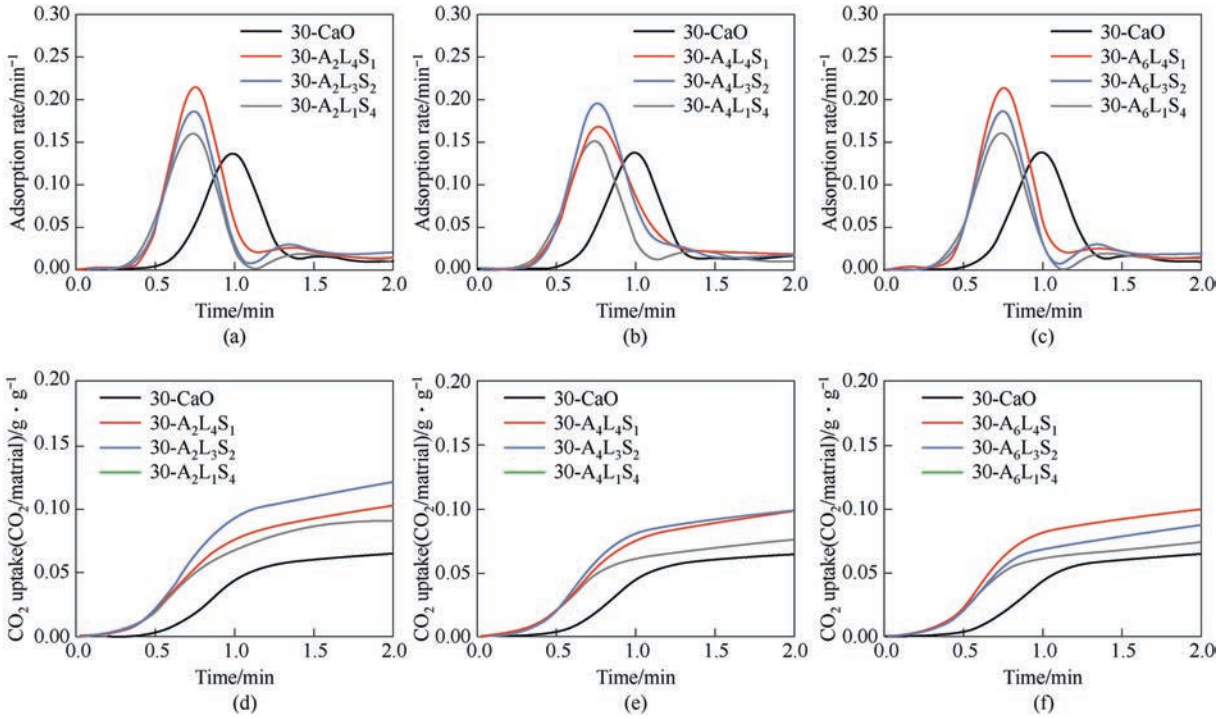

Fig. 7. Under mild conditions, Carbonation kinetics of commercial CaO and nine steel slag-derived hybrid materials during the final cycle: (a), (b), and (c) CO_2 sorption rate of the nine hybrid materials in the first 2 min, respectively; (d), (e), and (f) CO_2 sorption capacities of the nine hybrid materials in the first 2 min, respectively.

and pore volume, their results are displayed in Table 3. As the initial acid concentration rises, the BET specific surface area and BJH cumulative pore volume of the hybrid materials exhibit a gradual increment. Additionally, their average pore size generally shows an upward tendency along with the increase in the initial acid concentration. In the study of Tian *et al.* [53], it was shown that the amount and concentration of the added acetic acid affected the characteristics of the pore structure of the materials, and the pores of the materials are filled with a large number of acetic acid molecules and water molecules under the high concentration of acetic acid addition. It can be known that in the case of higher initial acid concentration, the steel slag derived hybrid material precursor contains higher acetic acid molecules and water molecules. After the hybrid material precursor has been calcined at 850 °C, the pore-forming ability of the calcium-based hybrid material is improved because more acetic acid and water molecules would be volatilized by the heat. This process improved the pore-forming ability of the hybrid material, so that the pore structure of hybrid material can be improved.

The effect of slag doping ratio on porosity is opposite. With more steel slag doping, metal elements are leached out in large quantities and easily form compounds with Ca, such as $Ca_2Fe_2O_5$, which was proved to be an important bonding phase in sintered ores of ironmaking. $Ca_2Fe_2O_5$ can improve the strength and reducibility of sintered ores, covering the surface of the hybrid material, which enhances the stability but leads to the clogging of some of the pore sizes [54]. The specific surface area and average pore size of sample $A_2L_1S_4$ were the lowest among the nine samples, which may be due to the low acid concentration and excessive steel slag components in the preparation of sample $A_2L_1S_4$. It is worth mentioning that $A_4L_3S_2$ has the specific BET surface area (9.8 $m^2 \cdot g^{-1}$) and pore volume (0.058 $cm^3 \cdot g^{-1}$) that rank third among the nine composites and CaO grain size of this material also has obvious advantages (69.3 nm being the second smallest). These data demonstrate that the material has abundant and high-density surface-active sites, which endow it with excellent sorption capacity and sorption rate [55,56].

Their sorption and desorption isothermal curves were all characterized by typical type IV isotherms (IUPAC classification) and H3 hysteresis loops, indicating the presence of mesopores in the hybrid material. As shown in Fig. 9(d)–(f), it is evident that the pore sizes of the samples are mostly within the mesopore range. Only a small number of pores are in the macropore region. Mesopores in greater quantity are beneficial for capturing carbon dioxide. Additionally, an appropriate quantity of macropores can effectively stabilize the structure of the hybrid material by preventing pore blockage during the cyclic tests. The coexistence of mesopores and macropores in the hybrid material is of crucial significance for enhancing the efficiency of hydrogen production during the biomass steam reforming process. Hence, this coexistence plays a vital role. The mesopores facilitate the sorption and diffusion of reactants, while the macropores help maintain structural integrity and prevent pore blockage, ensuring sustained catalytic activity throughout the process. This dual-porosity structure thus enhances the overall performance of the hybrid material in hydrogen production. It is noteworthy that with the increase in initial acid concentration, the sample is inclined to form larger pore sizes. In particular, A_2 and A_4 generate more mesopores, thereby widening their pore channels. This not only alleviates the adverse impacts caused by the volume changes resulting from calcium carbonate produced during the carbonation reaction (for instance, pore blockage and covering of catalytic active sites) but also is beneficial for the diffusion of CO_2. The pore size distribution of the $A_4L_3S_2$ material is significantly different from that of the other two materials synthesized with 4 $mol \cdot L^{-1}$ acid. It has a richer mesoporous structure and the pore sizes are generally larger. This further proves that it has a larger specific surface area, which is also conducive to gas diffusion and improves the sorption rate.

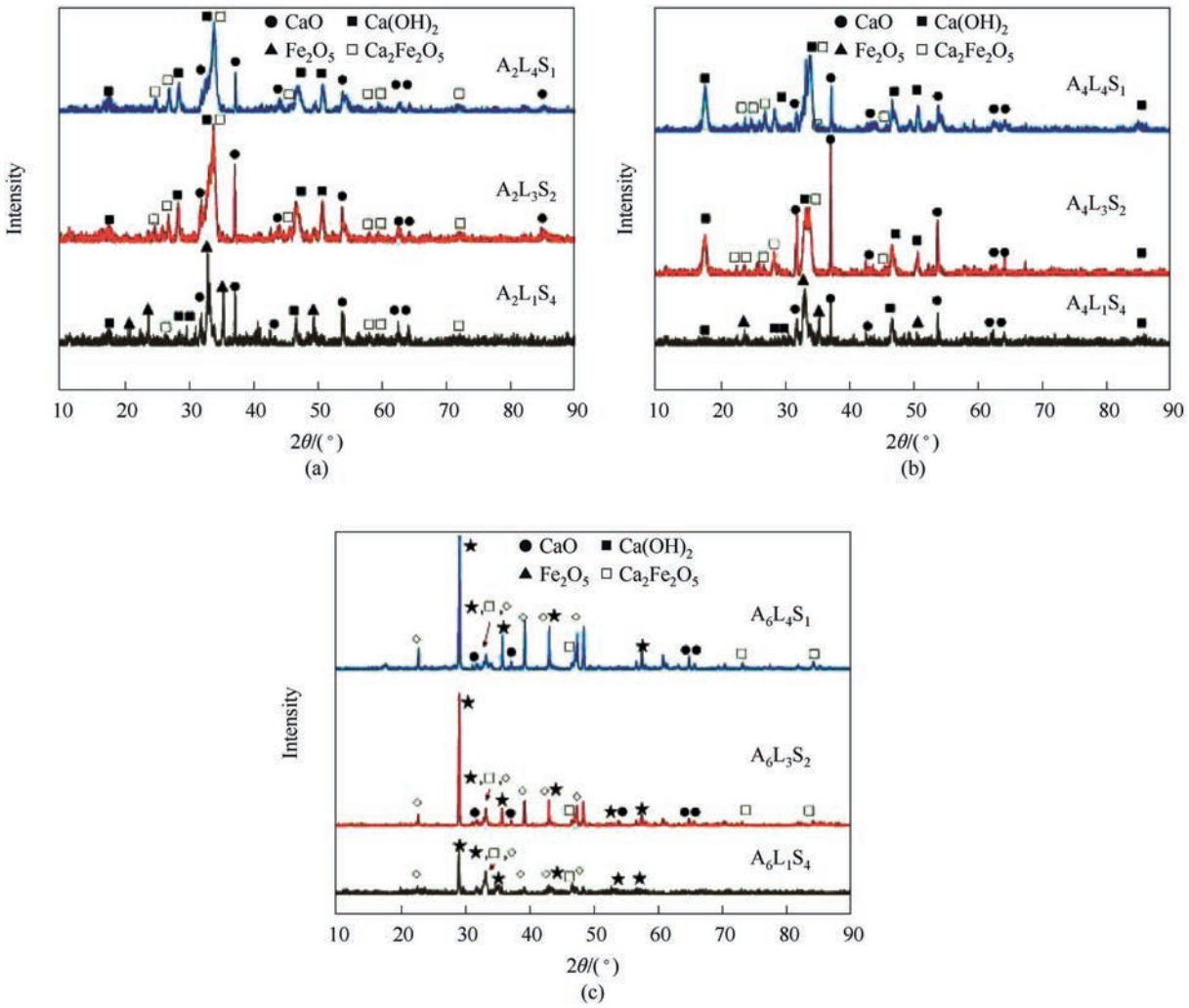

Fig. 8. X-ray diffraction patterns of steel slag-derived hybrid materials. (a) A_2 series; (b) A_4 series; (c) A_6 series.

Table 4
Composition of nine steel slag-derived hybrid materials (%, mass).

Sample	Composition						
	CaO	Fe_2O_3	SiO_2	Al_2O_3	MgO	MnO	Others
$A_2L_4S_1$	81.44	7.80	5.78	1.21	0.82	0.30	2.66
$A_2L_3S_2$	75.14	11.53	6.65	1.21	1.08	0.48	3.91
$A_2L_1S_4$	28.63	27.80	26.56	4.65	1.85	1.12	9.39
$A_4L_4S_1$	77.42	9.60	6.81	1.35	1.00	0.41	3.41
$A_4L_3S_2$	60.24	29.27	1.03	0.84	0.76	1.13	6.73
$A_4L_1S_4$	33.28	33.05	16.64	3.31	2.18	1.31	10.23
$A_6L_4S_1$	77.57	10.77	6.19	1.32	0.51	0.40	3.24
$A_6L_3S_2$	54.06	31.92	4.91	1.01	0.63	1.08	6.38
$A_6L_1S_4$	35.67	34.88	11.67	2.83	2.27	1.41	11.28

3.4.3. SEM analysis

As can be seen from the electron microscope images, the surface of the hybrid material is rough and porous, which is very different from commercial calcium oxide (Fig. 10(a)–(d)). After testing under mild conditions, Fig. 10((e)–(h)) original small particles in the hybrid material were all agglomerated into one larger particle due to sintering. Among them, commercial CaO had the most severe particle agglomeration, leading to the loss of a large number of pore channels. The steel slag doping significantly mitigated the effect of sintering and kept most of the pore channels open. $A_4L_3S_2$ performed well in terms of total sorption, partly due to the fact that it possessed enough steel slag doping to form more inert components with high Tammann temperatures, which were able to prevent the growth of the CaO particles and restrain their agglomeration, forming rigid barriers between the CaO grains. High initial acid concentration, which tended to form the inert components was also partially responsible for the improved stability [57]. The agglomeration phenomenon of $A_2L_4S_1$ and

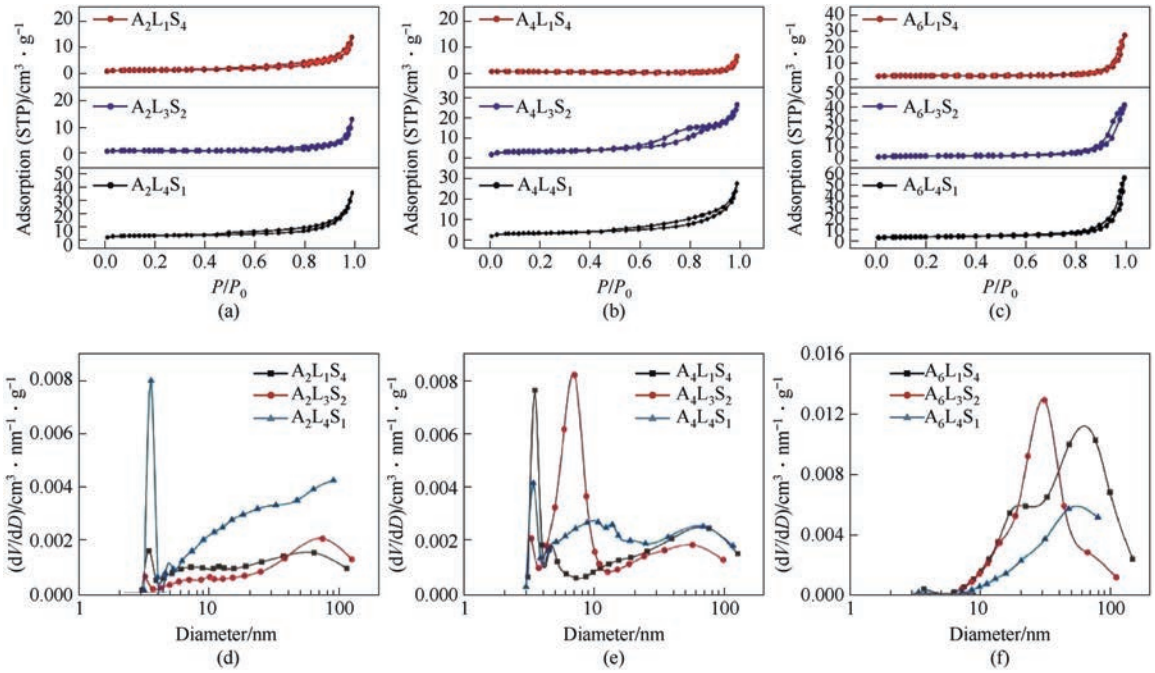

Fig. 9. N_2 physis-sorption isotherms (a–c) and pore size distributions (d–f) of steel slag-derived hybrid materials.

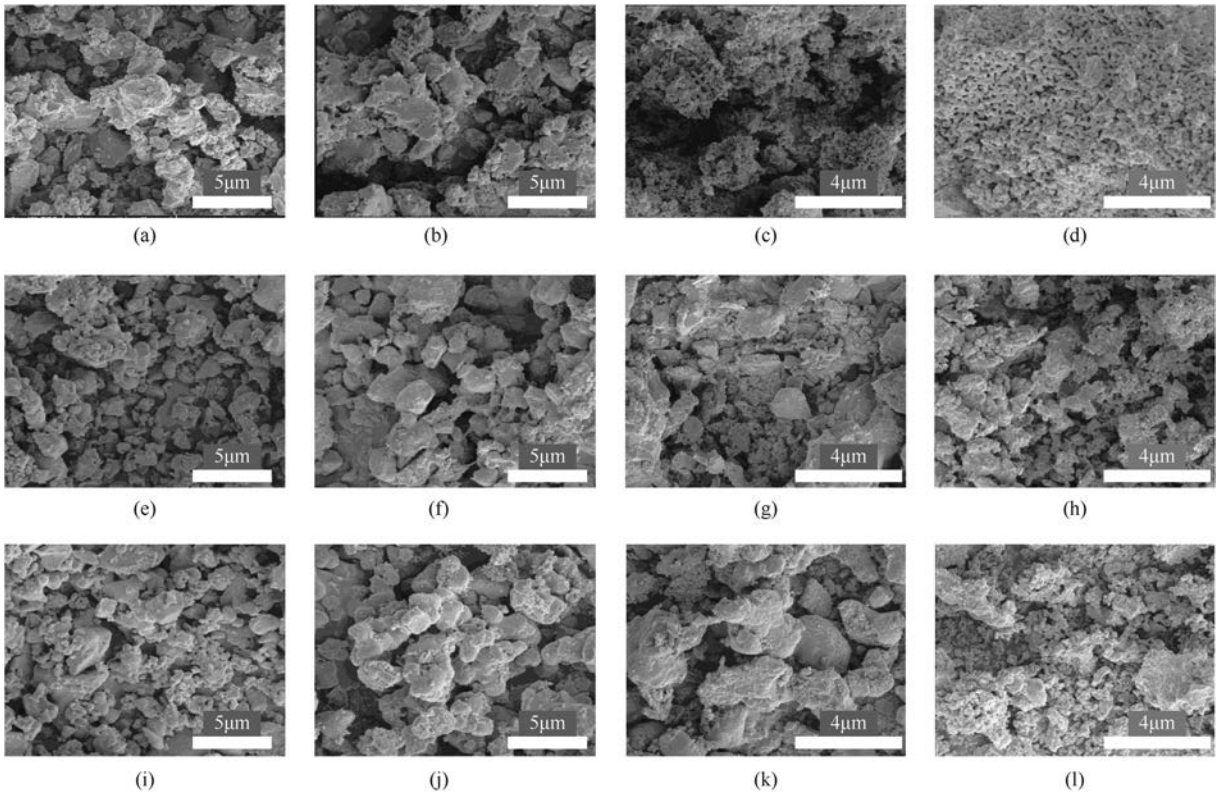

Fig. 10. SEM images of steel slag-derived hybrid materials: before use (a–d); after 30 cycles under mild testing conditions (e–h); after 30 cycles under severe testing conditions (i–l): (a), (e) and (i) for CaO; (b), (f) and (j) for $A_2L_4S_1$; (c), (g) and (k) for $A_4L_3S_2$; (d), (h) and(l) for $A_6L_1S_4$.

$A_4L_3S_2$ after sorption was significantly improved compared to that of CaO, and $A_2L_4S_1$ and $A_4L_3S_2$ still have better fluffy structure and pores, which further affirms the stability of them. After the sorbent was tested under harsh conditions (Fig. 10(i)–(l)), the agglomeration of particles was significantly more severe than that after the test under mild conditions, resulting in the loss of a large number of pores. This also explains the reason for the rapid deactivation of the sorbent under harsh conditions.

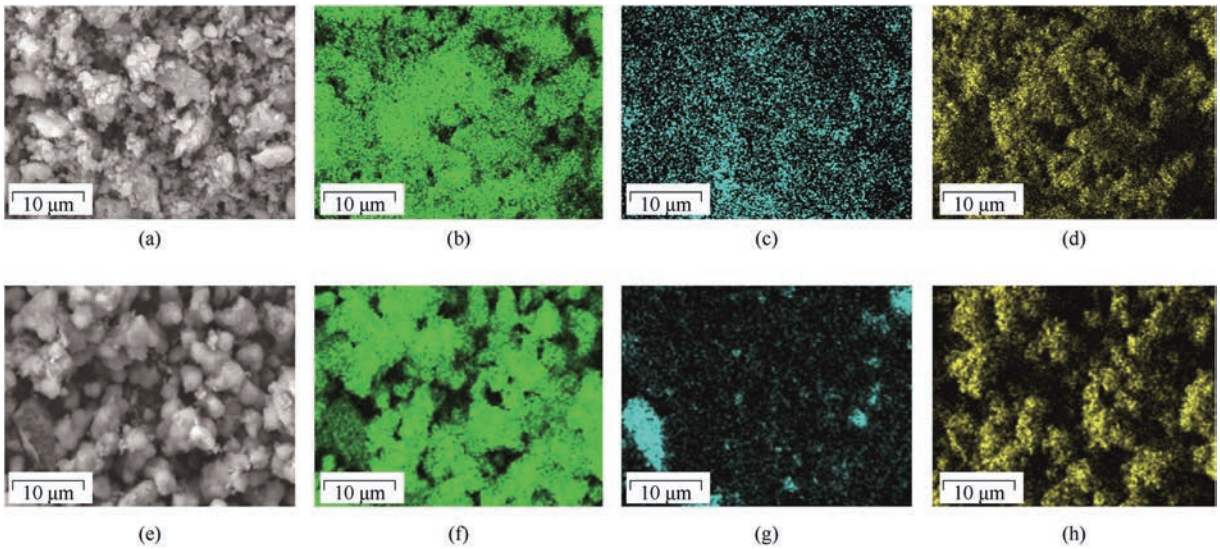

Fig. 11. SEM-EDS Mapping of calcium (b and f), iron (c and g) and oxygen (d and h)composition in fresh and used $A_4L_3S_2$ hybrid materials: (a)–(d) for fresh $A_4L_3S_2$ hybrid materials; (e)–(h) for $A_4L_3S_2$ hybrid materials after 30 cycles under mild testing conditions.

Table 5
Outcomes of the proximate and ultimate analysis on pine wood shaving (%, mass).

Proximate analysis①			Ultimate analysis②		
Volatile matter	83.62	±2.28	C	48.53	±0.17
Moisture	4.61	±1.13	H	7.66	±0.56
Fixed carbon	10.83	±2.98	O	43.67	±1.24
Ash	0.94	±0.36	N	0.14	±0.03

① As received condition.
② Dry and ash-free condition.

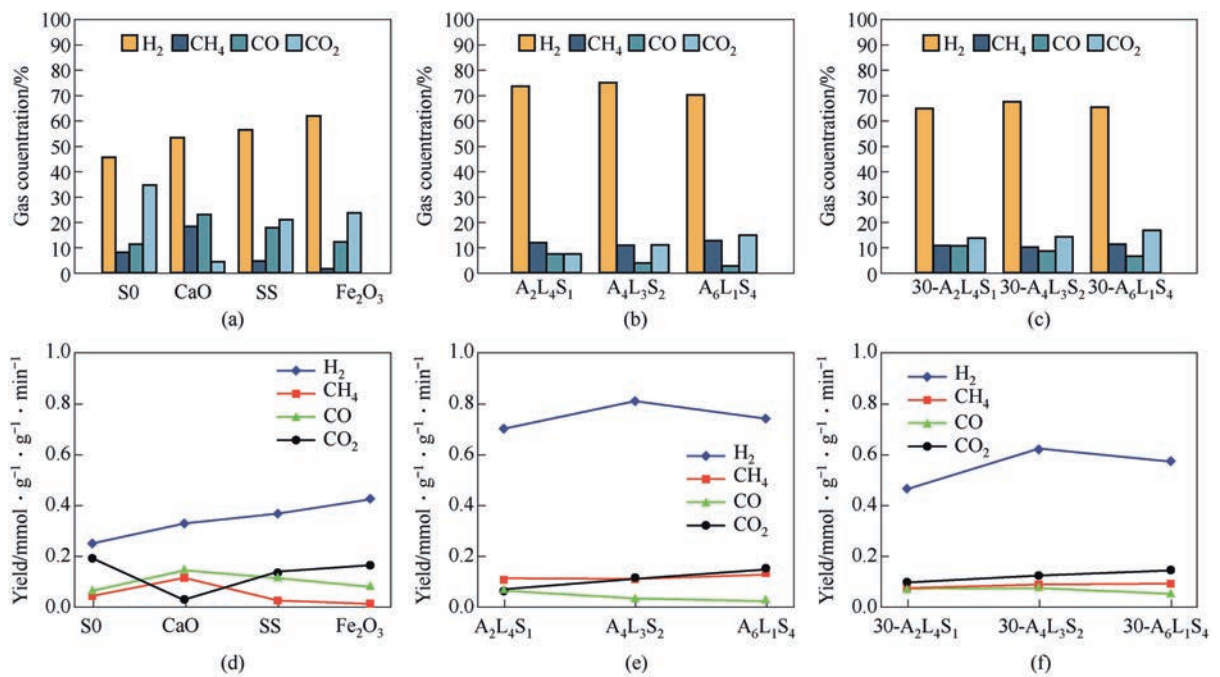

Fig. 12. The effect of hydrogen production by sorption-enhanced biomass steam reforming: Gas concentration (a–c) and yield (d–f) for control group and fresh preferred steel slag-derived hybrid materials; (a) and (d) the control group: S0, without adding any materials; CaO, commercial CaO; SS, steel slag; Fe_2O_3, commercial AR Fe_2O_3.; (b) and (e) fresh hybrid materials; (c) and (f) used hybrid materials.

Table 6
Performance summary and comparison of three hybrid materials.

Sample	Total adsorption capacity in 30 cycles/g·g^{-1}	Maximum capacity attenuation after 30 cycles/%	Hydrogen purity/%	Hydrogen yield/mmol· g^{-1}·g^{-1}·min^{-1}
CaO	3.67	72.41	45.58	0.26
$A_2L_4S_1$	4.44	37.09	73.42	0.71
$A_4L_3S_2$	4.14	21.87	74.57	0.82
$A_6L_1S_4$	2.78	8.68	70.12	0.75

EDS mapping (Fig. 11) shows that Ca, Fe and O elements are uniformly distributed on the surface of $A_4L_3S_2$ samples. This indicates that the hybrid materials, catalysts, stabilizers and other components in the material form a good mixing state at the nanoscale, which is conducive to the synergistic effect between the components and jointly promote the performance of the material. It is clearly observable from the figure that after 30 cycles, most of the aggregated Ca forms small particles, which further proves that the doping of steel slag is effective in preventing the aggregation of calcium oxide particles.

3.5. Analysis of hydrogen production results

The biomass used in the experiment is pine wood shaving. The results of proximate and ultimate analysis of pine sawdust are shown in Table 5.

Fig. 12 illustrates the effects of the fresh steel slag-derived hybrid materials and the steel slag-derived hybrid materials after 30-cycles of CO_2 sorption on sorption-enhanced pine wood shaving steam reforming. As can be seen, the hydrogen purity in the production of the blank group of S0 is the lowest. This is mainly because the reforming reaction is difficult to proceed completely without the presence of a catalyst. The hydrogen purity of the group with CaO is significantly higher than that of the blank group. However, without the assistance of a catalyst, it doesn't have an obvious advantage in terms of hydrogen purity. Steel slag has a little sorption ability and catalytic ability, so it performs relatively well in hydrogen production. But the sorption ability of the raw steel slag without treatment is weak, and it cannot sorb a sufficient amount of CO_2 quickly during the process, resulting in a relatively high concentration of CO_2 (21.07%) remaining in the syngas. Therefore, it is unable to push the WGS reaction thoroughly in the forward direction. Fe_2O_3 is one of the typical catalysts for the reforming reaction. Therefore, it can significantly increase the hydrogen concentration in the reactants and has a remarkable catalytic effect. In addition, it can be observed that the methane content in the CaO group is relatively high. This is because the sorption of CO_2 by CaO promotes the WGS reaction, resulting in the production of more hydrogen. However, it also promotes the methanation reaction, which is why the increase in the content of H_2 is not significant. In contrast, the methane content in both the SS group and the Fe_2O_3 group is relatively low. This is due to the fact that they act as catalysts, facilitating the breaking of the chemical bonds in CH_4. This explanation accounts for the obvious improvement in the purity of H_2 in these two groups. It can be clearly seen that the addition of the hybrid materials has led to a significant improvement in both the purity and yield of hydrogen. Fresh $A_2L_4S_1$ showed the most excellent CO_2 sorption performance in the hydrogen production part, significantly and reducing the CO_2 content in the syngas to only 7.2% and the CO_2 yield is 0.12 mmol·g^{-1}·g^{-1}·min^{-1}, which is consistent with the results of the previous CO_2 sorption experiments. Fresh $A_4L_3S_2$ showed a slightly lower CO_2 sorption performance but achieved approximately 74.57% hydrogen purity and the highest hydrogen yield (0.818 mmol g^{-1}·g^{-1}·min^{-1}), making it the best among the three hybrid materials. Additionally, the CO content in the syngas was observed to be relatively low, attributed to its good catalytic and CO_2 sorption capacities, with only 10.89% CO_2 content. This facilitated the WGS reaction, achieving a high CO conversion rate [58]. These results further confirm the optimal combination of active component CaO and catalytic component Fe in $A_4L_3S_2$. Although fresh $A_6S_1L_4$ performed poorly in the CO_2 sorption experiments, the presence of a substantial amount of Fe as a catalytic component still enabled the syngas to achieve a hydrogen purity of 70.12%.

As shown in Fig. 12(c) and (d), the hydrogen production enhancing effect of the three hybrid materials declined to some extent after 30 cycles of CO_2 sorption. However, the hydrogen purity and yield of hydrogen in the syngas remained at a relatively high level. An increase in CO and CO_2 content in the syngas was observed for all three hybrid materials. This can be attributed to sintering of the hybrid materials, which led to a reduction in active sorption sites and catalytic sites within the materials. Consequently, the CO_2 sorption capacity of the materials decreased, hindering the timely removal of CO_2 from the reaction gases and weakening the enhancement effect of the reaction [59]. Moreover, it can be seen from Fig. 11(g) that the Fe element shows relatively concentrated aggregation, which indicates that its sintering is rather serious. This will lead to the reduction of catalytic performance and also explains the decline in the hydrogen production purity and hydrogen yield of the materials after 30 cycles.

Table 6 shows the properties of three hybrid materials. Due to the extremely obvious attenuation of its maximum sorption capacity during 30 cycles, CaO has insufficient sorption capacity for long-term cycling. Moreover, because it has no catalytic ability for the reforming reaction, the purity and yield of the obtained hydrogen are both low. The $A_2L_4S_1$ material has the best CO_2 sorption capacity. And since it contains only a small amount of Fe_2O_3 as a catalyst, the hydrogen production effect is significantly improved compared with CaO. The $A_4L_3S_2$ material performs well in both CO_2 sorption capacity and hydrogen production, and its cycling stability is significantly higher than that of $A_2L_4S_1$. By observing the data of the $A_6L_1S_4$ material, it can be seen that although its total sorption capacity is 2.78 g·g^{-1}, which is relatively low among the four materials, the maximum capacity attenuation rate after 30 cycles is only 8.68%, showing a significant advantage in cyclic stability.

In comparison, CaO is at a disadvantage in terms of cyclic stability and hydrogen production ability; $A_2L_4S_1$ has the core advantage of sorption capacity, and its hydrogen production effect has showed a breakthrough compared with CaO; $A_4L_3S_2$ achieved a better balance among sorption, hydrogen production, and cyclic stability; $A_6L_1S_4$ relies on outstanding cyclic stability. Therefore, it can be concluded that when synthesizing the sample, retaining at least more than 60% of the CaO component is the key to ensuring the sorption capacity. Meanwhile, a certain amount (20% to 30%) of Fe_2O_3 should be doped to act as an inert component and a catalytic component.

In addition, the initial acid concentration for preparing the material should not be too high ($\geq$6 mol·L^{-1} for acetic acid). On the one hand, it will cause excessive dissolution of irrelevant

components from the steel slag. On the other hand, it would leach out more CaO to combine with metal components, resulting in poor CO_2 sorption capacity.

4. Conclusions

This study successfully synthesized a catalyst-sorbent hybrid functional material using steel slag and limestone and demonstrated its excellent performance in multi-cycle CO_2 sorption experiments and the enhancement of pine wood shaving gasification for hydrogen production. The experiments showed that the hybrid material exhibited outstanding calcium conversion and anti-sintering properties, significantly outperforming commercial CaO. Among them, $A_4L_3S_2$ achieved a total CO_2 sorption capacity of 4.14 $g \cdot g^{-1}$ under mild conditions across 30 cycles, with CO_2 sorption capacity only decreasing to 3.81 $g \cdot g^{-1}$ after 30 cycles. In hydrogen production experiments, the steel slag-based materials significantly increased H_2 purity. For instance, $A_4L_3S_2$ achieved an H_2 purity of 74.57% and yield of 0.818 $mmol \cdot g^{-1} \cdot g^{-1} \cdot min^{-1}$ while reducing CO_2 concentration to 10.89% in first 10 min. The material's porous structure and anti-sintering properties ensured long-term stability. Microscopic analysis revealed that inert components (Fe_2O_3/$Ca_2Fe_2O_5$, *etc.*) effectively prevented particle aggregation and pore collapse at high temperatures. This study not only provides a new pathway for the resource utilization of steel slag but also reduces the cost of catalyst-sorbent materials, paving the way for industrial applications of biomass gasification hydrogen production. Relying on the low-cost steel slag, this material has both high sorption stability and anti-sintering properties. After being applied in the process of enhanced sorption biomass reforming to produce hydrogen, the sorbent that has lost its activity after multi-cycles, can be directly recycled as a raw material back to the blast furnace or converter for steelmaking, forming a closed loop of “solid waste resource utilization - enhanced sorption biomass reforming — waste recycling”. This provides an industrial-grade “low-cost, easy-to-promote, zero-waste” scalable path for CO_2 capture and hydrogen production.

CRediT Authorship Contribution Statement

Zechen Zhang: Writing — original draft, Project administration, Formal analysis, Visualization, Investigation. Tanzila Anjum: Writing — review & editing, Methodology. Yinxiang Wang: Project administration, Methodology. Yucen Meng: Methodology. Tianheng Qin: Methodology. Ye Shui Zhang: Methodology, Funding acquisition. Yutao Zhang: Methodology. Aimin Li: Supervision. Guozhao Ji: Writing — review & editing, Supervision, Project administration, Funding acquisition, Writing — original draft, Resources, Investigation, Formal analysis.

Declaration of Competing Interest

The authors declare that they have no known competing financial interests or personal relationships that could have appeared to influence the work reported in this paper.

Acknowledgements

This work was funded by the National Key Research and Development Program of China (2025YFE0109700), Open Foundation of Key Laboratory of Industrial Ecology and Environmental Engineering, MOE (KLIEEE-22-07) and UK Research and Innovation (UKRI) under the UK government's Horizon Europe funding guarantee [EP/Y036751/1].

Co-funded by the European Union (HyWay: 101130009). Views and opinions expressed are however those of the author(s) only and do not necessarily reflect those of the European Union or the Research Executive Agency. Neither the European Union nor the Research Executive Agency can be held responsible for them.

References

[1] Y. Zhou, R.Y. Li, Z.X. Lv, J. Liu, H.J. Zhou, C.M. Xu, Green hydrogen: a promising way to the carbon-free society, *Chin. J. Chem. Eng.* 43 (2022) 2–13.
[2] S. Niaz, T. Manzoor, A.H. Pandith, Hydrogen storage: materials, methods and perspectives, *Renew. Sustain. Energy Rev.* 50 (2015) 457–469.
[3] S. Sorrell, Reducing energy demand: a review of issues, challenges and approaches, *Renew. Sustain. Energy Rev.* 47 (2015) 74–82.
[4] M. Amin, H.H. Shah, A.G. Fareed, W.U. Khan, E. Chung, A. Zia, Z.U. Rahman Farooqi, C. Lee, Hydrogen production through renewable and non-renewable energy processes and their impact on climate change, *Int. J. Hydrogen Energy* 47 (77) (2022) 33112–33134.
[5] A. Yagmur Goren, I. Dincer, A. Khalvati, A comprehensive review on environmental and economic impacts of hydrogen production from traditional and cleaner resources, *J. Environ. Chem. Eng.* 11 (6) (2023) 111187.
[6] S. Latreche, N. Boutarek-Zaourar, I. Bencherifa, F. Messaoud, M. Trari, Electrochemical performance of NiAl-activated cathode for green hydrogen production, *Chin. J. Chem. Eng.* 75 (2024) 290–298.
[7] B. Wang, R. Xiao, H.Y. Zhang, An overview of bio-oil upgrading with high hydrogen-containing feedstocks to produce transportation fuels: chemistry, catalysts, and engineering, *Curr. Org. Chem.* 23 (7) (2019) 746–767.
[8] H. Aki, I. Sugimoto, T. Sugai, M. Toda, M. Kobayashi, M. Ishida, Optimal operation of a photovoltaic generation-powered hydrogen production system at a hydrogen refueling station, *Int. J. Hydrogen Energy* 43 (32) (2018) 14892–14904.
[9] C.Y. Li, S.W. Chu, C.Y. Ho, H.J. Chang, T.J. Wan, A comprehensive review of critical factors affecting green ammonia synthesis by electrochemical process, *J. Environ. Chem. Eng.* 12 (6) (2024) 114454.
[10] P.E. Dodds, I. Staffell, A.D. Hawkes, F. Li, P. Grünewald, W. McDowall, P. Ekins, Hydrogen and fuel cell technologies for heating: a review, *Int. J. Hydrogen Energy* 40 (5) (2015) 2065–2083.
[11] Y. Wan, Z.M. Zhou, Z.M. Cheng, Hydrogen production from steam reforming of methanol over $CuO/ZnO/Al_2O_3$ catalysts: catalytic performance and kinetic modeling, *Chin. J. Chem. Eng.* 24 (9) (2016) 1186–1194.
[12] F. Li, D. Liu, K. Sun, S.H. Yang, F.Z. Peng, K.X. Zhang, G.D. Guo, Y. Si, Towards a future hydrogen supply chain: a review of technologies and challenges, *Sustainability* 16 (5) (2024) 1890.
[13] M.T. Dunstan, F. Donat, A.H. Bork, C.P. Grey, C.R. Müller, CO_2 capture at medium to high temperature using solid oxide-based sorbents: fundamental aspects, mechanistic insights, and recent advances, *Chem. Rev.* 121 (20) (2021) 12681–12745.
[14] Y.X. Gong, J.S. Yao, P. Wang, Z.X. Li, H.J. Zhou, C.M. Xu, Perspective of hydrogen energy and recent progress in electrocatalytic water splitting, *Chin. J. Chem. Eng.* 43 (2022) 282–296.
[15] Z.L. Wang, C.W. Wu, X.L. Wang, M.Z. Xie, Y.F. Li, Z.H. Zhan, Y. Shuai, Ultradurable solar-driven seawater electrolysis for sustainable hydrogen production, *Adv. Funct. Mater.* 35 (9) (2025) 2416014.
[16] A. Hosseinzadeh, J.L. Zhou, X.W. Li, M. Afsari, A. Altaee, Techno-economic and environmental impact assessment of hydrogen production processes using bio-waste as renewable energy resource, *Renew. Sustain. Energy Rev.* 156 (2022) 111991.
[17] P. Zhou, I.A. Navid, Y. Ma, Y. Xiao, P. Wang, Z. Ye, B. Zhou, K. Sun, Z. Mi, Solar-to-hydrogen efficiency of more than 9% in photocatalytic water splitting, *Nature* 613 (7942) (2023) 66–70.
[18] M. Li, Y.S. Zhang, S. Cheng, B. Qu, A. Li, F. Meng, G. Ji, The impact of heating rate on the decomposition kinetics and product distribution of algal waste pyrolysis with in-situ weight measurement, *Chem. Eng. J.* 457 (2023) 141368.
[19] N. Muradov, Low to near-zero CO_2 production of hydrogen from fossil fuels: status and perspectives, *Int. J. Hydrogen Energy* 42 (20) (2017) 14058–14088.
[20] A. Midilli, H. Kucuk, M.E. Topal, U. Akbulut, I. Dincer, A comprehensive review on hydrogen production from coal gasification: challenges and opportunities, *Int. J. Hydrogen Energy* 46 (50) (2021) 25385–25412.
[21] M. Ayesha, A.H. Khoja, F.A. Butt, U. Sikandar, A.H. Javed, S.R. Naqvi, I.U. Din, M.T. Mehran, Sorption enhanced steam reforming of methane over waste-derived CaO promoted MgNiAl hydrotalcite catalyst for sustainable H_2 production, *J. Environ. Chem. Eng.* 10 (3) (2022) 107651.
[22] E. Peralta-Reyes, D. Vizarretea-Vásquez, R. Natividad, A. Aizpuru, E. Robles-Gómez, C. Alanis, A. Regalado-Méndez, Electrochemical reforming of glycerol into hydrogen in a batch-stirred electrochemical tank reactor equipped with stainless steel electrodes: parametric optimization, total operating cost, and life cycle assessment, *J. Environ. Chem. Eng.* 10 (4) (2022) 108108.
[23] K.K. Moses, A. Aliyu, A. Hamza, I.A. Mohammed-Dabo, Recycling of waste lubricating oil: a review of the recycling technologies with a focus on catalytic cracking, techno-economic and life cycle assessments, *J. Environ. Chem. Eng.* 11 (6) (2023) 111273.

[24] J.S. Qu, J.B. Zhang, H.Q. Li, S.P. Li, D. Shi, R.Q. Chang, W.F. Wu, G.Y. Zhu, C.N. Yang, C.Y. Wang, Occurrence, leaching behavior, and detoxification of heavy metal Cr in coal gasification slag, *Chin. J. Chem. Eng.* 58 (2023) 11–19.
[25] H. Ishaq, C. Crawford, Towards less carbon-intensive blue hydrogen: integrated natural gas reforming and CO_2 capture approach, *J. Environ. Chem. Eng.* 13 (2) (2025) 115043.
[26] S.K. Dash, S. Chakraborty, D. Elangovan, A brief review of hydrogen production methods and their challenges, *Energies* 16 (3) (2023) 1141.
[27] M. Voldsund, K. Jordal, R. Anantharaman, Hydrogen production with CO_2 capture, *Int. J. Hydrogen Energy* 41 (9) (2016) 4969–4992.
[28] S. Manigandan, J.I. Ryu, T.R. Praveen Kumar, M. Elgendi, Hydrogen and ammonia as a primary fuel–A critical review of production technologies, diesel engine applications, and challenges, *Fuel* 352 (2023) 129100.
[29] L.S. Wang, Z.D. Du, J. Feng, X.L. Shi, W.Y. Li, Thermal coupling study during the co-processing of coal and biomass in the lab-scale adiabatic reactor, *Chin. J. Chem. Eng.* 78 (2025) 303–313.
[30] M. Mujtaba, L. Fernandes Fraceto, M. Fazeli, S. Mukherjee, S.M. Savassa, G. Araujo de Medeiros, A. do Espírito Santo Pereira, S.D. Mancini, J. Lipponen, F. Vilaplana, Lignocellulosic biomass from agricultural waste to the circular economy: a review with focus on biofuels, biocomposites and bioplastics, *J. Clean. Prod.* 402 (2023) 136815.
[31] A. Capa, Y.L. Yan, F. Rubiera, C. Pevida, M.V. Gil, P.T. Clough, Process simulations of high-purity and renewable clean H_2 production by sorption enhanced steam reforming of biogas, *ACS Sustainable Chem. Eng.* 11 (12) (2023) 4759–4775.
[32] H. Zhu, Y. Wang, X.L. Zheng, P. Li, Y.Y. Zhu, X.B. Li, Sol-gel auto-combustion synthesis of bimetallic Pt-Co/Al_2O_3 catalysts for hydrogen production *via* acetic acid steam reforming, *J. Environ. Chem. Eng.* 12 (3) (2024) 112758.
[33] M. Cortazar, S.Z. Sun, C.F. Wu, L. Santamaria, L. Olazar, E. Fernandez, M. Artetxe, G. Lopez, M. Olazar, Sorption enhanced ethanol steam reforming on a bifunctional Ni/CaO catalyst for H_2 production, *J. Environ. Chem. Eng.* 9 (6) (2021) 106725.
[34] D.D. Zhou, Y.X. Wang, Z.C. Zhang, Y.T. Zhang, A.M. Li, J.D. Luan, G.Z. Ji, Vacuum assisted desorption of sodium zirconate sorbent for enhancing cyclic stability in pre-combustion CO_2 capture, *Carbon Capture Sci. Technol.* 13 (2024) 100277.
[35] P. Suriya, S.S. Xu, S.Z. Ding, S. Chansai, Y.L. Jiao, J. Hurd, D. Lee, Y.X. Zhang, C. Hardacre, P. Reubroycharoen, X.L. Fan, Ethanol steam reforming over Ni/ZSM-5 nanosheet for hydrogen production, *Chin. J. Chem. Eng.* 67 (2024) 247–256.
[36] D.D. Zhou, Y.X. Wang, M.Z. Memon, W. Fu, Z.Q. Wu, S.J. Sheng, H.M. Zhang, G. Z. Ji, The effect of Na_2ZrO_3 synthesis method on the CO_2 sorption kinetics at high temperature, *Carbon Capture Sci. Technol.* 3 (2022) 100050.
[37] Y.S. Wang, N. Li, M.Q. Chen, D.F. Liang, C. Li, Q. Liu, Z.L. Yang, J. Wang, Glycerol steam reforming over hydrothermal synthetic Ni-Ca/attapulgite for green hydrogen generation, *Chin. J. Chem. Eng.* 48 (2022) 176–190.
[38] H.M. Sun, J.Q. Wang, J.H. Zhao, B.X. Shen, J. Shi, J. Huang, C.F. Wu, Dual functional catalytic materials of Ni over Ce-modified CaO sorbents for integrated CO_2 capture and conversion, *Appl. Catal. B Environ.* 244 (2019) 63–75.
[39] J. Saupsor, S. Wongsakulphasatch, P. Kim-Lohsoontorn, P. Bumroongsakulsawat, W. Kiatkittipong, S. Ratchahat, S. Charojrochkul, J.L. Gong, S. Assabumrungrat, Fe_2O_3/CaO-Al_2O_3 multifunctional catalyst for hydrogen production by sorption-enhanced chemical looping reforming of ethanol, *Biomass Convers. Biorefin.* 13 (10) (2023) 8651–8668.
[40] C. Quan, M.C. Wang, N.B. Gao, T.H. Yang, R.D. Li, *In situ* adsorption of CO_2 to enhance biomass gasification for hydrogen production using Ca/Ni based composites, *J. Energy Inst.* 108 (2023) 101229.
[41] J.Y. Wang, P.F. Wu, Y.L. Wei, Q.F. Zhao, P. Ning, Y.M. Huang, S.K. Wen, J.Y. Xu, Q. Wang, Study of calcium-based CO_2 sorbent with high cycling stability derived from steel slag and its anti-sintering mechanism, *J. CO2 Util.* 66 (2022) 102279.
[42] S.C. Tian, J.G. Jiang, F. Yan, K.M. Li, X.J. Chen, Synthesis of highly efficient CaO-based, self-stabilizing CO_2 sorbents *via* structure-reforming of steel slag, *Environ. Sci. Technol.* 49 (12) (2015) 7464–7472.
[43] B.X. Zhang, Y.M. Chen, B.K. Kang, J.F. Qian, X. Chuai, R.F. Peng, Z.P. Li, F.Q. Guo, W.J. Yan, J.Y. Zhang, Hydrogen production *via* steam reforming of coke oven gas enhanced by steel slag-derived CaO, *Int. J. Hydrogen Energy* 45 (24) (2020) 13231–13244.
[44] S.C. Tian, K.M. Li, J.G. Jiang, X.J. Chen, F. Yan, CO_2 abatement from the iron and steel industry using a combined Ca–Fe chemical loop, *Appl. Energy* 170 (2016) 345–352.
[45] Y.X. Wang, H. Zhou, D.D. Yao, G. Olguin, H.X. Ding, B.Y. Qu, W.S. Xie, Z.G. Fu, Y. Guo, X. Wang, A.M. Li, G.Z. Ji, Ni-CaO-$CaZrO_3$ bi-functional materials for high purity hydrogen production *via* sorption enhanced steam reforming of ethanol, *J. Clean. Prod.* 446 (2024) 141397.
[46] S. Ibrahim, B.H. Hameed, F.A. Almomani, Review on recent progress in post-combustion carbon dioxide capture using carbonaceous and non-carbonaceous materials in fixed-bed adsorption column, *J. Environ. Chem. Eng.* 13 (1) (2025) 114952.
[47] C.S. Martavaltzi, A.A. Lemonidou, Parametric study of the CaO–$Ca_{12}Al_{14}O_{33}$ synthesis with respect to high CO_2 sorption capacity and stability on multicycle operation, *Ind. Eng. Chem. Res.* 47 (23) (2008) 9537–9543.
[48] M. Zhao, J. Shi, X. Zhong, S.C. Tian, J. Blamey, J.G. Jiang, P.S. Fennell, A novel calcium looping absorbent incorporated with polymorphic spacers for hydrogen production and CO_2 capture, *Energy Environ. Sci.* 7 (10) (2014) 3291–3295.
[49] M.A. Carreon, V.V. Guliants, Ordered meso- and macroporous binary and mixed metal oxides, *Eur. J. Inorg. Chem.* 2005 (1) (2005) 27–43.
[50] I. Zamboni, C. Courson, A. Kiennemann, Fe-Ca interactions in Fe-based/CaO catalyst/sorbent for CO_2 sorption and hydrogen production from toluene steam reforming, *Appl. Catal. B Environ.* 203 (2017) 154–165.
[51] F.J. Wang, S.Y. Chen, S.B. Chen, P.X. Yuan, L.B. Duan, W.G. Xiang, CO_2 capture and H_2 production performance of calcium-based sorbent doped with iron and cerium during calcium looping cycle, *process*, *Saf. Environ. Prot.* 188 (2024) 1175–1190.
[52] S.C. Tian, J.G. Jiang, F. Yan, K.M. Li, X.J. Chen, V. Manovic, Highly efficient CO_2 capture with simultaneous iron and CaO recycling for the iron and steel industry, *Green Chem.* 18 (14) (2016) 4022–4031.
[53] C.Y. Ding, X.W. Lv, G. Li, C.G. Bai, S.W. Xuan, K. Tang, X.M. Lv, Isothermal reduction of powdery $2CaO{\cdot}Fe_2O_3$ and $CaO{\cdot}Fe_2O_3$ under H_2 atmosphere, *Int. J. Hydrogen Energy* 43 (1) (2018) 24–36.
[54] H.X. Guo, X.C. Kou, Y.J. Zhao, S.P. Wang, Q. Sun, X.B. Ma, Effect of synergistic interaction between Ce and Mn on the CO_2 capture of calcium-based sorbent: textural properties, electron donation, and oxygen vacancy, *Chem. Eng. J.* 334 (2018) 237–246.
[55] M. Zhao, X. He, G.Z. Ji, Y.Q. Song, X. Zhao, Zirconia incorporated calcium looping absorbents with superior sintering resistance for carbon dioxide capture from *in situ* or *ex situ* processes, *Sustain. Energy Fuels* 2 (12) (2018) 2733–2741.
[56] M. Zhao, Y.Q. Song, G.Z. Ji, X. Zhao, Demonstration of polymorphic spacing strategy against sintering: synthesis of stabilized calcium looping absorbents for high-temperature CO_2 sorption, *Energy Fuels* 32 (4) (2018) 5443–5452.
[57] S. Teir, S. Eloneva, C.J. Fogelholm, R. Zevenhoven, Dissolution of steelmaking slags in acetic acid for precipitated calcium carbonate production, *Energy* 32 (4) (2007) 528–539.
[58] Q.X. Lu, K. Wu, Z.T. Zha, Y.N. Ma, Z.F. Ge, H.Y. Zhang, A review on potential applications of Fe/Ni/Ca in biomass catalytic reforming to produce hydrogen, *Fuel* 365 (2024) 131158.
[59] J.T. Chen, J.X. Wang, H.W. Jiang, X.L. Zuo, X. Yang, Effects of over-sintering on cyclic calcination and carbonization of natural limestone for CO_2 capture, *Processes* 12 (9) (2024) 1926.